Li et al. PhotoniX (2021) 2:11
https://doi.org/10.1186/s43074-021-00032-2

PhotoniX

REVIEW Open Access

Subwavelength silicon photonics for on-chip mode-manipulation

Chenlei Li[1], Ming Zhang[1,2], Hongnan Xu[1], Ying Tan[1,2], Yaocheng Shi[1,2] and Daoxin Dai[1,2*]

* Correspondence: dxdai@zju.edu.cn
[1]Centre for Optical and Electromagnetic Research, State Key Laboratory for Modern Optical Instrumentation, Zhejiang Provincial Key Laboratory for Sensing Technologies, International Research Center for Advanced Photonics, College of Optical Science and Engineering, Zhejiang University, Hangzhou 310058, China
[2]Ningbo Research Institute, Zhejiang University, Ningbo 315100, China

Abstract

On-chip mode-manipulation is one of the most important physical fundamentals for many photonic integrated devices and circuits. In the past years, great progresses have been achieved on subwavelength silicon photonics for on-chip mode-manipulation by introducing special subwavelength photonic waveguides. Among them, there are two popular waveguide structures available. One is silicon hybrid plasmonic waveguides (HPWGs) and the other one is silicon subwavelength-structured waveguides (SSWGs). In this paper, we focus on subwavelength silicon photonic devices and the applications with the manipulation of the effective indices, the modal field profiles, the mode dispersion, as well as the birefringence. First, a review is given about subwavelength silicon photonics for the fundamental-mode manipulation, including high-performance polarization-handling devices, efficient mode converters for chip-fiber edge-coupling, and ultra-broadband power splitters. Second, a review is given about subwavelength silicon photonics for the higher-order-mode manipulation, including multimode converters, multimode waveguide bends, and multimode waveguide crossing. Finally, some emerging applications of subwavelength silicon photonics for on-chip mode-manipulation are discussed.

Keywords: Subwavelength, Silicon photonics, Mode manipulation, Polarization, Multimode, Waveguide

Introduction

Silicon photonics has been developed very successfully and become very promising for various applications due to its unique advantages [1–5], such as a wide transparent window, an ultra-high index-contrast and the CMOS (complementary metal-oxide-semiconductor) compatibility. Currently great efforts have been made to further improve the performances for silicon photonic devices to satisfy the demands in practical applications. Generally speaking, it is often desired to develop ultra-compact silicon photonic devices with ultra-low excess losses (ELs), ultra-high extinction ratios (ERs), ultra-low crosstalk (CT), ultra-broad bandwidths, as well as large fabrication tolerances, etc. The realization of such high-performance silicon photonic devices with large fabrication tolerances is a vital step for developing large-scale photonic integrated circuits (PICs), as noticed. In this paper, we concern high-performance silicon

photonic devices for on-chip mode-manipulation, which plays an important role in various photonic systems for many applications.

In particular, we focus on the on-chip mode-manipulation with two popular subwavelength photonic waveguide structures developed in the past years. *One* is silicon hybrid plasmonic waveguides (HPWGs) [6–10], which is fully SOI (silicon-on-insulator)-compatible and has strong field enhancement in the low-index nano-slot region as well as very strong polarization-dependence. Meanwhile, the propagation loss due to the metal absorption in HPWGs is at the order of 0.01 dB/μm, which is much lower than those traditional metal nanoplasmonic waveguides. In particular, on-chip photonic devices assisted locally by HPWGs can have acceptably low losses and ultra-compact footprints [8]. As a result, in the past decade various HPWGs with modified structures have been proposed very popularly for realizing ultra-high integrated density [6–10], which are very attractive for the development of integrated photonics. The *other* one is silicon subwavelength-structured waveguides (SSWGs), such as subwavelength-grating (SWG) waveguides [11–13], in which the equivalent refractive index can be modified freely by adjusting the duty-circle according to the effective medium theory. When using SSWGs, there are lots of opportunity to effectively manipulate the properties of the guided-modes, including the effective indices, the mode fields, the birefringence, and the mode dispersion. More importantly, SSWGs usually have very low propagation losses of about 2 dB/cm [11–13], which is similar to the loss of regular strip waveguides. Therefore, SSWGs have attracted intensive attention in recent years. As it might be noticed, the fabrication for both HPWGs and SSWGs is more difficult than regular SOI strip waveguides due to the deep subwavelength feature size. It even more challenging for the fabrication of metal strips in HPWGs, and thus there are less experimental results for HPWGs than SSWGs. Nevertheless, these two types of subwavelength photonic waveguides are still very attractive and popular regarding their unique properties. Besides, the nanofabrication is expected to be improved further in the near future. Thus, it will be more and more popular to introduce special subwavelength photonic waveguides, which can effectively manipulate the properties of the guided-modes and help the future development of silicon photonic integrated circuits.

As it is well known, initially silicon photonics has been developed well with the design rule defined by the singlemode condition. In this case, the fundamental-mode manipulation is recognized as the basic physical mechanism for realizing many silicon photonic devices, including the modal field profiles, the spot sizes, the evanescent fields, the effective indices, the waveguide dispersion, and the birefringence. In particular, the polarization-mode manipulation has attracted intensive attention because it is very important for various photonic systems, like polarization-transparent PICs [14–17], coherent optical communications [18, 19] and quantum communication [20], etc. Definitely the polarization-mode manipulation relies on high-performance polarization-handling devices, including polarizers, polarization-beam splitters (PBSs), polarization rotators (PRs), and polarization-splitter-rotators (PSRs). In the past decade, high-performance polarization-handling devices on silicon have been developed with great efforts by utilizing the ultra-high birefringence of silicon nanophotonic waveguides. As demonstrated recently, the device performances can possibly be very excellent by introducing novel device structures/schemes as well as novel subwavelength silicon photonic waveguides with extraordinary birefringence, which is reviewed in section 2.1. In

addition, power coupling/splitting of the fundamental mode also plays very important roles in many optical systems, and we focus on two representative fundamental devices for silicon photonics in section 2.2. One is ultra-broadband 2×2 power splitters for optical interference systems, and the other one is broadband mode converters for efficient coupling between a singlemode fiber and a silicon-on-insulator (SOI) stirp waveguide.

More recently, multimode silicon photonics has been very attractive by introducing higher-order modes to enable the mode-division multiplexing (MDM) technology, so that multi-channel data communications can be achieved even with a single wavelength-carrier. Furthermore, some special photonic devices can be realized flexibly when higher-order modes are introduced. As a result, higher-order mode manipulation has been paid more and more attention. Great progresses have been achieved on multimode silicon photonics in the past few years [21–24]. In this paper, we focus on two major parts of higher-order-mode manipulation. One is for higher-order mode coupling/conversion, including multi-channel mode-selective couplers, ultra-compact mode generators/exchangers, and 2×2 multimode power splitters, as reviewed in section 3.1. The other one is for higher-order-mode propagation, including sharp multimode waveguide bends (MWBs) and multimode waveguide crossings (MWCs), as reviewed in section 3.2. Next, the emerging applications of subwavelength silicon photonics would be reviewed in section. Finally, we give a summary and an outlook subwavelength silicon photonics for on-chip mode-manipulation.

Subwavelength silicon photonics for the fundamental-mode manipulation

In order to satisfy enormous demands of ultra-high link capacity in various scales of optical interconnects, advanced (de) multiplexing technologies have been used very widely. Among them, wavelength-division-multiplexing (WDM) and polarization-division-multiplexing (PDM) are recognized as the most mature technologies. For WDM systems, including dense WDM with many wavelength-channels ($N\sim10^2$) and coarse WDM with large channel-spacing (e.g., $\Delta\lambda_{ch}\sim20$ nm), it is becoming very desired to develop low-loss and low-crosstalk silicon photonic devices works in an ultra-broad wavelength-band as required. For PDM systems, polarization management always plays an important role as one of the most important technologies. Thus, it is desired to develop high-performance on-chip polarization-handling devices, including polarizers, polarization-beam splitters (PBSs), polarization rotators (PRs), and polarization-splitter-rotators (PSRs). These on-chip polarization-handling devices also paly very important roles to enable the polarization-diversity technology for many other systems, like polarization-transparent PICs [14–17], coherent optical transceivers [18, 19] and quantum communications [20], etc. Generally speaking, polarization-handling devices are usually desired to have low ELs and high ERs in an ultra-broad wavelength-band for various applications (including WDM optical interconnects).

The key for the realization of such high-performance photonic devices is to effectively manipulate the fundamental mode of TE- and TM-polarizations (i.e., the TE_0 and TM_0 modes), and great efforts have been made by introducing subwavelength silicon photonic waveguides in the past years. In the following parts, a review is given for recent progresses of on-chip polarization-handling devices as well as power couplers/splitters with novel structural designs based on subwavelength silicon photonic waveguides.

High-performance on-chip polarization-handling devices

On-chip polarization-handling devices for the TE_0/TM_0-mode manipulation have been developed successfully worldwide by using subwavelength silicon photonic waveguides in the past years and have been playing important roles for many applications [14–23]. The key elements for polarization-handling mainly include polarizers, PBSs, and PRs/PSRs. In the following parts, we give a review for the newly-developed high-performance polarization-handling devices with subwavelength silicon photonic waveguides.

Polarizers

On-chip polarizers are often needed to achieve linearly polarized light with a high ER. Currently many silicon-based on-chip polarizers with decent performances have been reported [24–54]. Basically speaking, a polarizer can be realized by manipulating the polarization-dependence of the propagation loss [24, 25], the cut-off condition [26–29], or the field profiles of the guided-modes in optical waveguides [30, 31]. For example, an on-chip polarizer was realized with the TM_0-TM_1 coupling in an asymmetric directional coupler (ADC) [24], which enables a high ER of >15 dB in a broad wavelength-band over 80 nm. In order to achieve compact and broadband high-performance polarizers, great efforts have been made in recent years. In particular, the special structures based on SSWGs [26–31] as well as HPWGs [32–54] provide promising approaches for realizing ultra-short optical polarizers, as summarized in Table 1.

In [28], an ultracompact and low-loss TM-pass polarizer on silicon was proposed and demonstrated experimentally by using an SWG waveguide, which is one of the most popular SSWGs, as shown in Fig. 1(a). Here the SWG waveguide was designed to support Bloch mode for TM polarization so that the incident TM-polarized light goes through the SWG waveguide with a very low EL. On the other hand, for TE polarization, the SWG waveguide works as a Bragg-grating reflector and consequently the incident TE-polarized light is reflected efficiently, which strongly depends on the period number N of the grating. For the fabricated ~9-μm-long polarizer with N=20, the polarization ER is ~27 dB and the EL is ~0.5 dB at the central wavelength 1550 nm experimentally. The bandwidth for achieving a polarization ER of >20 dB is about 60 nm (i.e., 1520-1580 nm). When increasing the period number to N=40, the measured polarization ER is up to 40 dB, which is not as high as the expected theoretical value 65 dB partially due to the setup limit. Similarly, an SWG-assisted TE-pass polarizer on silicon was demonstrated in [26], as shown in Fig. 1(b). In this design, the TM_0 mode is suppressed under the cutoff condition and thus has a high leakage loss. Meanwhile, the

Table 1 Comparison of the reported polarizers

Ref.	Year	Structure	Length (μm)	ER (dB)	EL (dB)	$BW_{ER>20dB}$ (nm)
[37]	2013	HPWG-	<4	12	<1	100
[28]	2014	SWG	~9	>20	<1	~60
[26]	2015	SWG	60	~30	~0.4	>100
[48]	2016	HPWG-	30	28	0.1	>150
[32]	2017	HPWG-	2.5	>25	<1	/
[31]	2019	Metamaterial	13	>20	<1	>415

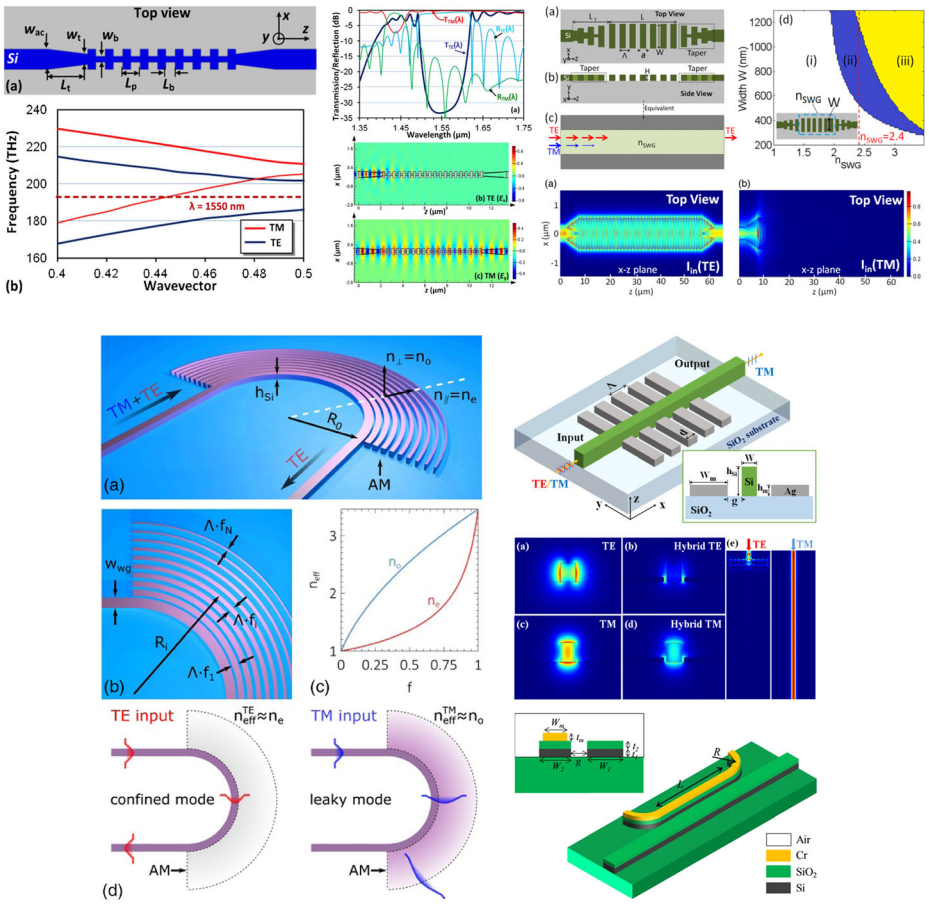

Fig. 1 Reported on-chip polarizers. **a** An SWG-assisted TM-pass polarizer [28]; **b** An SWG-assisted TE-pass polarizer [26]; **c** A polarizer based on a sharp SWG-assisted waveguide-bend [31]; **d** A polarizer based on an HPWG-assisted grating [37]; **e** A polarizer based on an HPWG-assisted ADC [48]; **f** A TM-Pass polarizer based on a hybrid plasmonic grating [32]

SWG waveguide supports low-loss propagation for the TE_0 mode. This TE-pass polarizer has a >200 nm bandwidth for achieving a polarization ER of 35 dB in theory. For the fabricated polarizer, the polarization ER is ~30 dB and the EL is ~0.4 dB in a broad wavelength range of 1470-1580 nm.

More recently, a TE-pass polarizer with an extremely broad bandwidth was proposed by using a 180° sharp waveguide-bend assisted with anisotropic SWG metamaterial structures [31], as shown in Fig. 1(c). In this structure, the sharp waveguide-bend has very strong polarization-dependent bending loss due to the anisotropy of the introduced SWG metamaterial structures. For TE polarization, the incident light can propagate through the sharp waveguide bend with very low EL because of the strong optical confinement enabled by the high effective-index-contrast. In contrast, the TM polarization mode in the sharp-bend is very lossy. For the fabricated polarizer, the EL is <1 dB and the polarization ER are >20 dB in an ultra-broad bandwidth of >415 nm, which is the first silicon on-chip polarizer covering all the optical communication-bands.

Another popular option for realizing compact on-chip polarizer is locally introducing a silicon HPWG [32–54], which is fully SOI-compatible and usually has a metal cap, a

silicon core as well as a SiO_2 insulator nano-layer between them, as proposed in 2009 [6]. As a kind of novel waveguide enabling subwavelength-scale optical field confinement, such an SOI-compatible silicon HPWG has very strong polarization dependence, which makes it very attractive for realizing ultra-compact polarization-handling devices (like polarizers) on silicon [40]. As shown in Fig. 1(d), in [37] a TM-pass polarizer was proposed by using a silicon side-grating with a narrow metal strip on the top. This grating was designed to work for TE polarization, so that the TE-polarized light is reflected efficiently when operating around the Bragg wavelength. On the other hand, the supported TM_0 hybrid plasmonic mode is "bounded" by the metal strip and is not influenced by the silicon side-grating structure almost. As a result, the TM-polarized light goes through the grating structure with low scattering/reflection losses. For the ~4.8-μm-long polarizer designed in [37], the ER is ~22 dB and the EL is ~1.1 dB at the central wavelength, while the bandwidth for achieving an ER of >20 dB is about 50 nm. Similarly, in [38] a TE-pass polarizer was proposed by using a silicon HPWG with a metal grating embedded in the low-index SiO_2 nano-slot layer. Here the metal grating was designed to reflect the TM-polarized light around the Bragg wavelength. Meanwhile, the metal grating introduces gentle influence to the propagation of the TE-polarized light. For the designed TE-pass polarizer in [38], the ER is ~18 dB, which is pretty high regarding that the device is as short as ~3.1 μm (for λ=1.55 μm).

In addition to the grating-based structure, an ADC consisting of an HPWG has also been used to realizing high-performance on-chip polarizer by utilizing the polarization-selective coupling in the ADC to remove the undesired polarized-light [48], as shown in Fig. 1(e). In this example, the ADC is designed according to the phase-matching condition, so that the TM_0 mode is cross-coupled from the SOI strip waveguide to the HPWG and then attenuated completely. Meanwhile, the TE_0 mode goes through the coupling region with a low EL because there is a significant mode-mismatching and no cross-coupling happens almost. For the fabricated 30-μm-long polarizer, the ER is >28 dB over the bandwidth of 150 nm. More importantly, this polarizer has a very low EL of <0.04 dB for the TE_0 mode. More recently, another low-loss and compact TM-pass polarizer was proposed with a metal grating-structure on silicon, as shown in Fig. 1(f) [32]. This polarizer is designed for TE polarization by taking the effective index and the mode overlap together into consideration, so that the incident TE_0 mode is blocked very efficiently. Meanwhile, the incident TM_0 mode can go through the grating structure without any notable EL. For the designed 2.5-μm-long polarizer, the ER is over 25 dB and the EL is less than 0.1 dB, which is comparable to pure-silicon devices.

Polarization-beam splitters (PBSs)

Currently many different structures have been proposed theoretically and demonstrated experimentally for realizing high-performance PBSs, including ADCs [55–77], multimode interference structures [78], grating-assistant structures [79], hybrid plasmonic Y-branches [80], SWG couplers [81–83]. Some of them have shown very high performances in a broad bandwidth, as reviewed in [21]. For example, as one of the best devices reported, a high-performance PBS based on cascaded bent directional couplers (DCs) was demonstrated recently with a low EL of <0.5 dB and a very high ER of >30 dB in a bandwidth of ~70 nm [61]. More importantly, this PBS has shown excellent

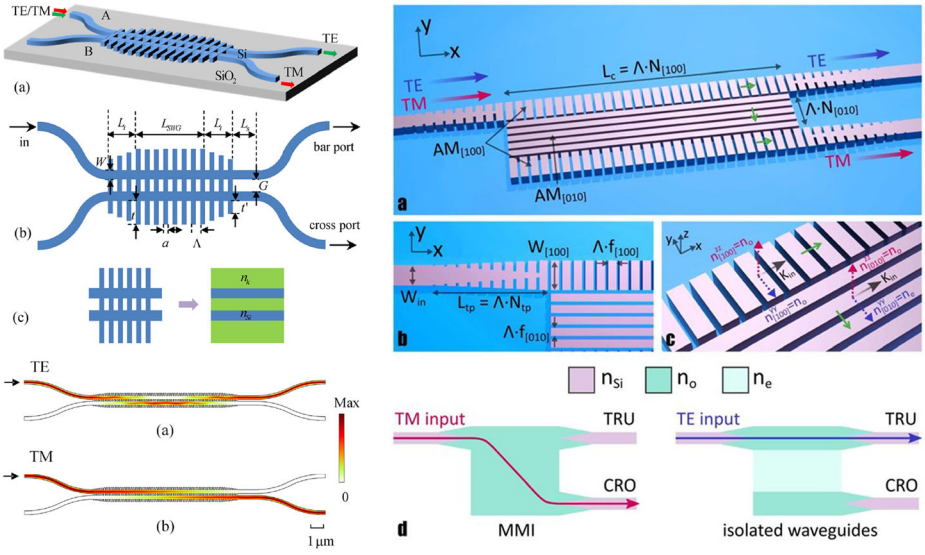

Fig. 2 **a** A PBS based on a straight DC assisted by SWG [82]; **b** A PBS based on anisotropic metamaterial [83]

fabrication tolerances. In order to achieve PBSs with an ultra-broad working bandwidth, some novel mechanisms should be introduced by using e.g. a coupling system with engineered waveguide dispersion, a mode evolution structure, etc.

As it is well known, an SWG waveguide can be treated as an equivalent waveguide with homogeneous refractive index in the corresponding regions. The birefringence and the dispersion for SWG waveguides can be manipulated flexibly through the refractive index engineering method. Therefore, SWG waveguides have been introduced as a typical SSWG to realize compact PBSs with high performances in a broad wavelength-band. In [82], an SWG-assisted straight DC was designed and demonstrated to realize a compact PBS [see Fig. 2(a)], which has an improved working bandwidth compared to the PBSs based on traditional straight DCs. Unfortunately, for this 40-μm-long PBS, the bandwidth for achieving ER>20 dB is about 28 nm, which is not sufficient yet for many applications. More recently, in [83] an on-chip silicon PBS using "material anisotropy" was proposed and demonstrated to break the bandwidth bottleneck. In particular, a slab with engineered anisotropy and dispersion was introduced, as shown in Fig. 2(b). The structure works as an MMI coupler for TM polarization and the launched TM-polarization mode outputs at the cross port when the length of the MMI region is chosen optimally according to the self-imaging theory. In contrast, the structure behaves like two decoupled straight waveguides for TE polarization and thus the launched TE-polarization mode outputs at the through port without any cross-coupling almost. For the fabricated PBS with a compact footprint as small as 12.3×1.9 μm^2, the ELs are less than 1 dB and the ERs are higher than 20 dB in a record working bandwidth of >200 nm.

Note that most of these PBSs were realized by using SOI photonic waveguides with a 220 nm-thick silicon core-layer (i.e., h_{co}=220 nm), in which case the ultra-high birefringence of the photonic waveguide enables the realization of high-performance PBSs. As it is well known, another popular option for the core-thickness in silicon photonics is h_{co}=340 nm [84], which potentially enables the propagation-loss reduction and gives

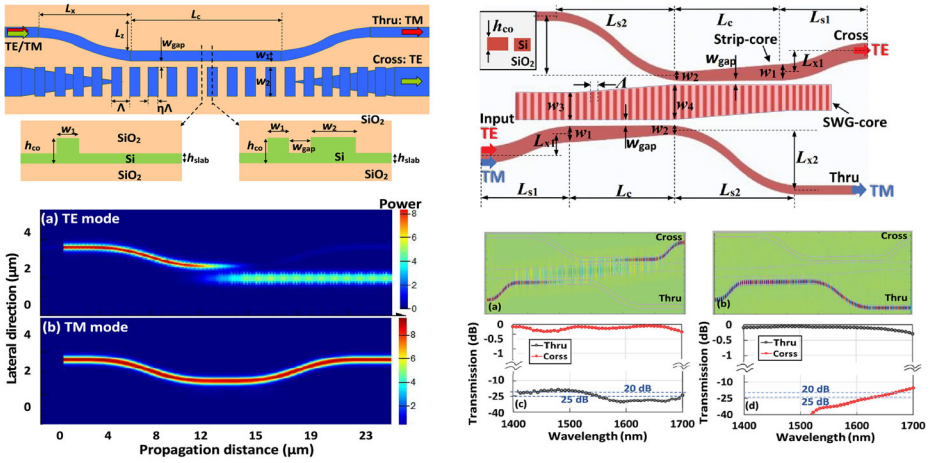

Fig. 3 PBSs with 340-nm-thick SOI waveguides. **a** A PBS based on an ADC consisting of a narrow SOI strip waveguide and a wide SWG waveguide [65]; **b** A PBS based on SWG-assisted dual-core adiabatic tapers [75]

more chance to achieve improved coupling efficiency for grating couplers [85]. Furthermore, a thicker silicon core-layer is usually desired for realizing silicon photonic modulators with higher modulation speed and higher efficiency [86]. When h_{co}=340 nm, the cross section of a singlemode SOI strip waveguide is usually chosen as ~340×340 nm^2, for which the birefringence is usually much less than that for the case of h_{co}=220 nm. As a result, it is not easy to realize a high-performance PBS with h_{co} =340 nm and those reported PBSs usually do not have excellent performance yet [65, 78, 82]. For example, a 570-μm-long PBS based on step-size MMIs was reported in [78], and the bandwidth for ER>15 dB is 20 nm only. Regarding that an SWG waveguide has very different birefringence from an SOI strip waveguide [65], it is possible to form an ADC by combining them together, as shown in Fig. 3(a). The ADC was designed optimally to make the phase-matching condition satisfied for TE polarization only. For the fabricated PBS with a ~2-μm-long coupling region, the ER is 15-30 dB and the EL is 0.2-2.6 dB for TE polarization while the ER is 20-27 dB and the EL is 0.3-2.8 dB for TM polarization in the wavelength range of 1520-1580 nm. Even though this PBS works better than those PBSs reported previously for the case of h_{co}=340 nm, it is desired to further improve the performance.

More recently, an ultra-broad PBS with high performances was proposed and realized for the case of h_{co}=340 nm by introducing cascaded SWG-assisted dual-core adiabatic tapers [75], as shown in Fig. 3(b). Each dual-core adiabatic taper consists of an SWG-core and a strip-core, whose widths are chosen optimally. According to the mode-evolution theory, the TE_0 mode launched from the input-waveguide can be converted gradually to the TE_0 mode at the cross output-waveguide. Meanwhile, the TM_0 mode stays in the through output-waveguide. In this way, the TE_0 and TM_0 modes can be separated easily. For the designed PBS with a 33.6-μm-long mode-evolution region, the ELs are <0.3 dB and the ERs are >20 dB for both TE- and TM-polarizations in an ultra-broad bandwidth from 1400 nm to 1700 nm in theory. For the fabricated PBS, the measured bandwidths for achieving ERs of ~20 dB and ~25 dB are 240 nm and 220 nm, while the 1-dB-bandwidth is as large as 230 nm, which are the largest bandwidths

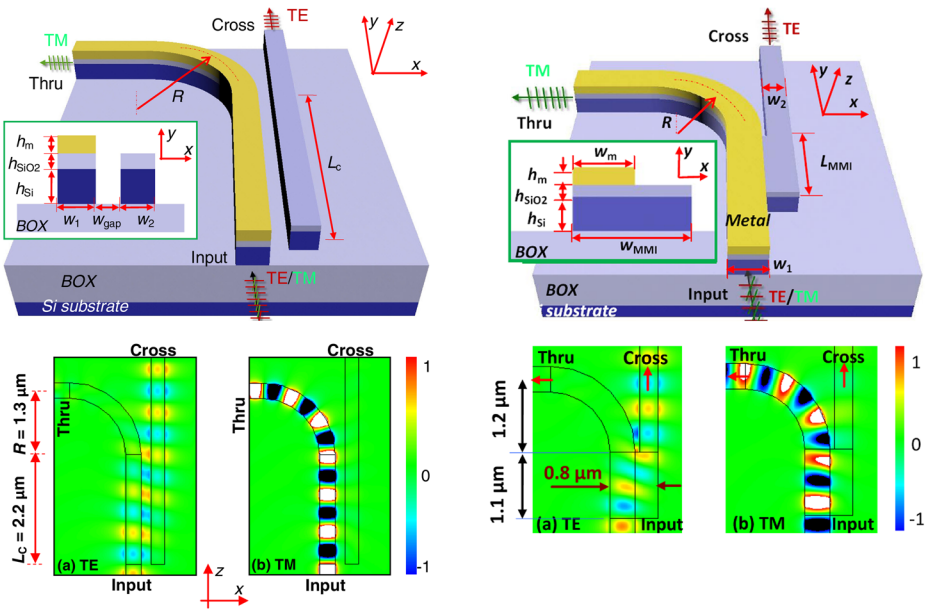

Fig. 4 a An ultracompact PBS based on an ADC assisted with a TM-type HPWG [88]; **b** An extremely-small PBS based on an MMI assisted with a TM-type HPWG [89]; **c** An ultracompact PBS based on an ADC assisted with a TE-type HPWG [90]

reported to date for the PBSs on silicon. Such an ultra-broadband high-performance PBS is useful for many applications.

When it is desired to realize extremely small PBSs, a potential design is to introduce silicon HPWGs locally [87–90]. A PBS can be realized with an ADC consisting of a silicon HPWG and an SOI strip waveguide. For example, in [87] a three-waveguide asymmetric coupling system consisting of two strip waveguides with a narrow HPWG between them was proposed for realizing ultra-compact PBSs. The core widths for the three waveguides in the coupling region was chosen optimally to make the TM_0 mode cross-coupled. For the designed PBSs, the total length (including the bending output section) is about 5-10 μm when the gap width is chosen as small as 100 nm. A simplified ADC consisting of an HPWG and an SOI strip waveguide was proposed to further reduce the PBS footprint, as shown in Fig. 4(a) [88]. For this PBS, these two waveguides in the coupling region of this ADC are designed optimally to make the phase-matching condition satisfied for TE polarization (instead of TM polarization). Furthermore, the sharp bending with a high polarization-dependent loss is connected at the through port to serve as a compact polarizer for enhancing the polarization ER. With this kind of two-waveguide ADC, the designed ultrasmall PBS has a footprint as small as ~1.9 × 3.7 μm^2 only (including the bent output section) even when the gap width is chosen as large as 200 nm to make the fabrication relatively easy. The designed PBS has a decent ER of ~12 dB over a ~120 nm bandwidth while the ELs for TE- and TM- polarizations are respectively 0.025 dB and 0.66 dB (which is mainly due to the metal absorption).

When using a metal-loaded MMI coupler proposed in [89], an extremely small PBS can be achieved, as shown in Fig. 4(b). This design is to introduce a metal strip covering the MMI section partially. When working for TM polarization, the TM_0 mode in the MMI section is excited dominantly due to the hybrid plasmonic effect, and thus no

MMI effect happens almost. As a result, the TM-polarized light outputs from the through port with low ELs. In contrast, when working with TE polarization, the metal strip does not strongly influence the mode excitation and the mode propagation in the MMI section because no hybrid plasmonic effect exists for TE-polarization modes. Thus, a mirror image can be formed at the cross port when the MMI length is chosen optimally. For the designed PBS, the MMI section is as short as only 1.1 μm, and the bandwidth for achieving an ER of >10 dB is ~80 nm. The ELs for TE- and TM-polarizations are respectively 0.32 dB and 0.88 dB, which are acceptable for most applications.

Since an HPWG is usually introduced locally to avoid high metal absorption, it is often desired to build a connection from an HPWG to an SOI strip waveguide. However, their TM-polarization modes usually have notable mismatching and some butt-coupling loss is introduced. In order to avoid a high butt-coupling loss, in [90] an ADC with a horizontal silicon HPWG for TE-polarization was proposed for realizing low-loss PBSs, as shown in Fig. 4(c). Here the structure is design to make the phase-matching condition satisfied for TM polarization, so that the incident TE_0 mode goes through the coupling region without any coupling almost while the TM_0 mode is cross-coupled efficiently. The cross-coupled TM_0 mode in the HPWG can be further butt-coupled efficiently to the TM_0 mode in the followed SOI strip waveguide because their TM_0 modes are well matched. For the designed PBS with a compact footprint of ~2.9×5.8 μm^2, the ELs are <0.7 dB for both polarizations while the ERs at the central wavelength are 21.3 dB and 17.9 dB for TM- and TE-polarizations, respectively.

Table 2 gives a summary for the ELs and ERs of the reported representative PBSs on silicon with h_{co}=220 nm as well as h_{co}=340 nm. It can be seen that there are only a few PBSs with a broad bandwidth of 100 nm or more for achieving ER>20 dB. For the SWG-assisted PBS based on a hetero-anisotropic slab, there are ultra-broad bandwidths for achieving ER >20 dB and ER>25 dB, i.e., $BW_{ER>20dB}$ =~200 nm and $BW_{ER>25dB}$ = ~170 nm [83], which is the highest one among the PBSs with h_{co}=220 nm. For the case of h_{co}=340 nm, the PBS based on SWG-assisted adiabatic dual-core tapers enables the highest bandwidths for achieving ER>20 dB and ER>25 dB, i.e., $BW_{ER>20dB}$ =~230 nm and $BW_{ER>25dB}$ =~200 nm [75]. On the other hand, it is noticed that there are very few on-chip PBSs with ER>30 dB, which is desired for the future applications. Currently the PBS based on cascaded bent DCs enables an ER of >30 dB in a bandwidth of ~70 nm, which is one of the best results. In the future, more efforts are needed for developing very-high-performance PBSs with an ultra-low EL (e.g., <0.5 dB) and ultra-high ER (e.g., >30 dB) in an ultra-broad bandwidth (e.g., >100 nm).

Polarization rotators (PRs) and polarization splitter-rotators (PSRs)

As it is well known, polarization rotators (PRs) and polarization splitter-rotators (PSRs) are very important for many polarization-related optical systems. In particular, PSRs enabling polarization-separation and polarization-rotation simultaneously are very attractive for high-density PICs. Even though the realization of waveguide-type PRs and PSRs is not easy because the optical axis of a planar optical waveguide cannot be rotated freely, great efforts have been made and several types of on-chip PRs/PSRs have been realized successfully [91–121]. For the realization of PRs/PSRs, one of the keys is

Table 2 Comparison of the reported PBSs

Ref.	Year	Structure	$BW_{EL<0.5dB}$ nm	$BW_{EL<1dB}$ nm	$BW_{EL<1.5dB}$ nm	$BW_{EL<2dB}$ nm	$BW_{ER>10dB}$ nm	$BW_{ER>15dB}$ nm	$BW_{ER>20dB}$ nm	$BW_{ER>25dB}$ nm	$BW_{ER>30dB}$ nm	Length
[61]	2017	Bent DC	85	140	/	/	/	/	135	95	70	20μm
[62] *	2018	ADC	/	80	/	/	/	/	100	60	20	29.4μm
[64] *	2018	MMI	/	/	/	/	/	/	20	/	/	600μm
[65]	2017	ADC/SWG	/	/	/	50	/	60	30	/	/	2μm
[75] *	2020	SWG	/	230	/	/	270	240	230	200	/	33.6μm
[76] *	2018	bent DC	/	/	40	/	70	40	/	/	/	1.5μm
[77] *	2019	adiabatic	/	120	/	175	/	/	175	120	/	11μm
[78]	2013	ADC	150	/	/	/	/	250	70	/	/	48μm
[79] *	2016	Grating	/	21	/	/	/	33	30	25	21	27.5μm
[80]	2016	HHPW				200	30					5μm
[82] *	2016	SWG	/	/	/	/	115	40	/	/		14.6μm
[83] *	2019	Metamaterial		200					200	175		12.2μm

Here the experiment results are indicated by *

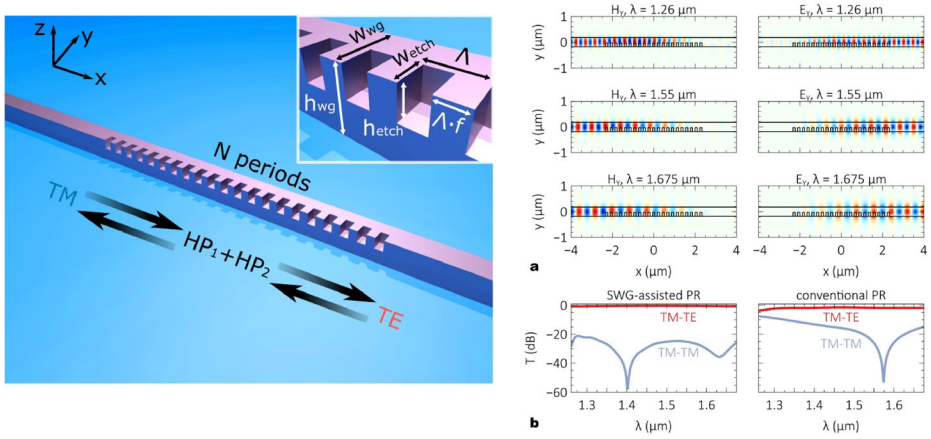

Fig. 5 An ultra-compact PR based on an SOI strip waveguide with SWG-assisted cut-corners [102]

to generate mode hybridness by introducing modified waveguide structures with cross-sectional asymmetry. Currently, the demonstrated PRs/PSRs are mainly realized by utilizing the hybridized-mode coupling in ADCs [91–98], the hybridized-mode interference in cut-cornered waveguides [99–102], and the hybridized-mode evolution in adiabatic tapers [103–108], as reviewed in [109]. In particular, the special structures based on SSWGs [110–113] as well as HPWGs [114–121] provide promising approaches for realizing high performance PRs/PSRs.

Basically speaking, the PRs/PSRs utilizing the hybridized-mode evolution are usually broadband but relatively long because the tapered structure should be adiabatic. When it is really desired to achieve compact and broadband PRs/PSRs, the utilization of hybridized-mode coupling in ADCs as well as hybridized-mode interference in cut-cornered waveguides might be preferred.

In [99], an ultra-short PR was proposed by utilizing a polarization-rotation section based on an SOI strip waveguide with a cut corner, in which two hybridized-modes are supported and two-mode interference happens. For this type of PR, the length of the polarization-rotation section is chosen optimally to be the beat length of two-mode interference. Such a PR can be even as short as ~7 μm with a broad bandwidth ~120 nm for high conversion efficiency >97% [99]. In order to achieve an ultrabroad bandwidth, more recently an SWG-assisted cut-corner was introduced [102], as shown in

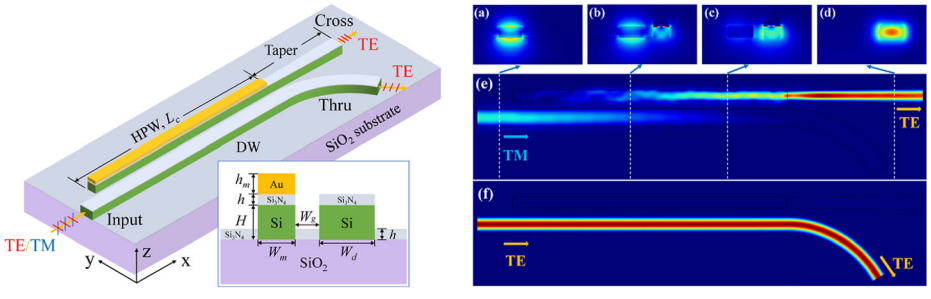

Fig. 6 A PSR with an ADC consisting of an HPWG and an SOI strip waveguide **a**, and the simulated light propagation in the design PSR for the incident TM_0 **b** and TE_0 **c** modes [117]

Table 3 Comparison of the reported PRs/PSRs

Ref.	Year	Structure	$BW_{EL<0.5dB}$	$BW_{EL<1dB}$	$BW_{EL<1.5dB}$	$BW_{EL<2dB}$	$BW_{ER>10dB}$	$BW_{ER>15dB}$	$BW_{ER>20dB}$	$BW_{ER>25dB}$	$BW_{ER>30dB}$	Length
[91] *	2016	bent WG	/	/	40nm	/	80nm	50nm	/	/	/	19.5μm
[101] *	2011	ADC	/	50nm	/	75nm	85nm	50nm	/	/	/	35μm
[102] *	2019	HPWG	/	/	/	35nm	/	/	35nm	/	/	7.7μm
[104]	2012	ADC	/	/	90nm	/	90nm	80nm	50nm	16nm	/	70μm
[105] *	2014	SWG	/	/	120nm	/	120nm	80nm	/	/	/	185μm
[106]	2019	adiabatic	/	415nm	/	/	/	300	220	/	/	240μm
[108]	2014	SWG	300nm	/	/	/	/	/	415nm	300nm	100nm	4.8μm

Here the experiment results are indicated by *

Fig. 5. In this design, the SWG structure was designed with engineered waveguide dispersion, so that the beat length of the two hybridized modes in the polarization-rotation section becomes wavelength-insensitive. The designed PR has a footprint as small as 4.8×0.34 μm^2. It is possible to achieve a high polarization ER of >20 dB and a low EL of <1 dB in an ultra-broad bandwidth of 1260-1675 nm, covering the O-, E-, S-, C-, L-, and U-bands.

As an alternative, utilization of an ADC with an HPWG provides another way for realizing compact PRs/PSRs. In [117], a compact PSR was realized with an ADC consisting of an HPWG and an SOI strip waveguide, as shown in Fig. 6(a)-(c). Here, in particular, a Si_3N_4 thin layer is introduced between the metal strip and the silicon strip. In this design, the waveguide dimensions are chosen carefully, so that the TM_0 mode in the SOI strip waveguide and the TE_0 mode in the HPWG are phase-matched, in which way efficient cross-polarization mode-coupling between them happens, as shown in Fig. 6(b)-(c). For the designed 7.7-μm-long PSR, the ERs for TM- and TE-polarizations are about 50 dB and 28 dB in theory at the central wavelength of 1550 nm, respectively. It enables a TM_0-TE_0 polarization-conversion efficiency of >95% within a bandwidth of 70 nm. The EL for the launched TE_0 mode is as low as 0.04 dB while the EL for the launched TM_0 mode is about 1.5 dB in theory, which is relatively high for the applications.

Table 3 gives a summary for the performances of the reported representative PRs and PSRs on silicon. Here the footprints of these PRs/PSRs are also shown. As it can be seen, the PRs/PSRs can be possibly as short as several microns, which are attractive for the future applications. Meanwhile, the bandwidth could be very large even for a high ER of >20 dB or more as well as a low EL of <1 dB or less when using some special designs [102]. On the other hand, note that most of these results are not experimental yet. Thus, more efforts should be made to fabricate these PRs/PSRs with precise nanofabrication technologies because their fabrication tolerance is usually small.

Subwavelength silicon photonics for power coupling/splitting of the fundamental mode

In addition to the polarization-manipulation, power coupling/splitting of the fundamental mode also plays very important roles in many optical systems. Here we focus two types of subwavelength silicon photonics for on-chip light manipulation of the fundamental mode. One is to realize an ultra-broadband 2×2 power splitter, which is the key element in many optical interference systems (e.g., Mach-Zehnder interferometers). Even though many structures have been demonstrated, one might notice that high-

Table 4 Comparison of the reported 3dB power splitters with silicon DCs

Ref	Year	Structures	L_c (μm)	L_t (μm)	Ratio (dB)	BW (nm)	EL (dB)
[136]	2015	Multi-section DC	31.4	41.4	3±1	88	<1
[139]	2016	SWG-DC	13.4	23.4	3±0.7	100	NA
[137]	2017	shallowly-etched DC	5	~550	NA	100	0.8
[130]	2018	Adiabatic DC	25	65	3±0.27	100	<0.74
[131]	2018	Adiabatic DC	35	NA	3±0.3	185	<0.11
[140]	2020	SWG-ADC	5.25	17.25	3±0.5	200	<1

L_c the length of the coupling region, L_t the total length, *BW* the bandwidth

performance 2×2 power splitters are still absent. The other is to realize broadband efficient power coupling between a singlemode fiber and an SOI stirp waveguide, which has been regarded as one of the most important parts for silicon photonics.

Ultra-broadband 2×2 optical power splitters for the fundamental mode

As it is well known, an optical power splitter is a key for separating and combining optical signals in PICs and have been used widely in many applications, such as optical switches, optical modulators, add-drop multiplexers, and optical phased array [122–125]. Currently there are three popular types of optical power splitters, which are based on DCs [126], MMI couplers [127] and Y-branches [128]. Among them, conventional DCs consisting of two identical straight waveguides are used widely due to the simplicity of the structural design and the fabrication process. However, the bandwidth is quite limited due to the strong wavelength-dependence of the evanescent coupling, which limits the applications in many broadband optical systems. Some methods have been proposed to enhance the operation bandwidth by minimizing the wavelength-dependence of the coupling systems [129–139], including adiabatic DCs [129–131], asymmetric DCs (ADCs) [132, 133], and multi-section DCs [134–136], as summarized in Table 4.

When utilizing adiabatic DCs, one can realize broadband power splitters, which usually requires to be long. For example, in [129] the adiabatic taper is as long as 100 μm. When using ADCs, one can obtain a compact footprint as well as a wavelength-insensitive power-splitting ratio. For example, in [133] the demonstrated power splitter works with a bandwidth of 100 nm ranging from 1500 nm to 1600 nm, which however is difficult to be extended further. For a traditional DC, it is also possible to be broadband by engineering the super-mode dispersion when some special structures are introduced [137–141]. As demonstrated in [137], the design using shallowly-etched rib waveguides with engineered supermode-dispersion of the DC is introduced, in which case more than one careful etching-steps are required. In recent years, SWGs have also been utilized to engineer the mode-dispersion of a symmetric DC for achieving improved operation bandwidths [138, 139]. In this case, only a single etching-step is needed. As shown in [138], the SWG-assisted DC is 19.2-μm-long and the imbalance is

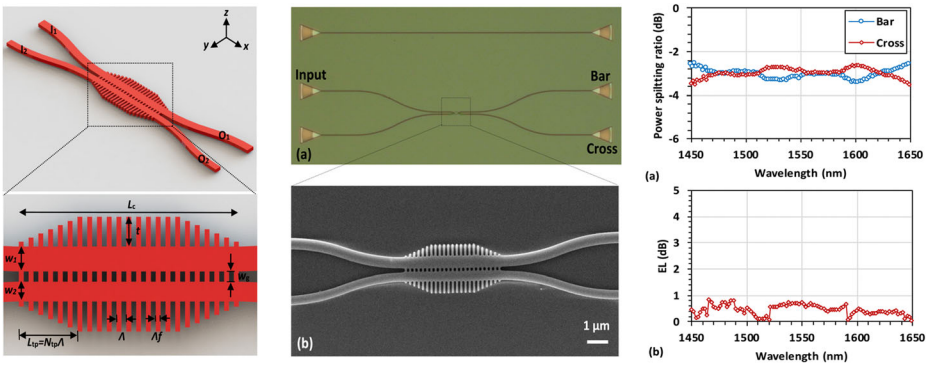

Fig. 7 a An ultra-broadband 2×2 3 dB power splitter using an SWG-assisted ADC; **b** SEM image of the fabricated SWG-assisted ADC; Measurement power splitting ratios **c** and ELs **d** for the fabricated SWG-assisted ADC [140]

≤0.6 dB in a 100 nm bandwidth. More recently, an ultra-compact broadband 2×2 3-dB power splitter based on an SWG-assisted ADC was proposed and demonstrated, as shown in Fig. 7(a)-(d). This ADC is designed to have a maximal coupling ratio around 50%, which is helpful to reduce the wavelength dependency of the 3 dB power-splitter [140]. Furthermore, the SWG structure inserted in the coupling region of the ADC is designed to engineer the mode-dispersion for further increasing the operation bandwidth. The SWG structure also helps reduce the coupling length and make the device very compact. For the designed splitter, the straight coupling region is as short as 5.2 μm and the bandwidth is as large as 300 nm (1400-1700 nm) for achieving an imbalance better than ±0.4 dB as well as an EL less than 0.33 dB for TE polarization. The experimental result verified that the fabricated coupler works well with a power splitting ratio better than 3 ± 0.5 dB and an EL less than 1 dB in the wavelength range from 1450 nm to 1650 nm, as shown Fig. 7(c)-(d). Such a broadband 2×2 3 dB power splitter is very helpful for achieving broadband MZI-based optical switches in the future.

High-efficiency fiber-chip couplers

Great efforts have been made for realizing efficient coupling between a singlemode fiber and an SOI strip waveguide, which is a fundamental prerequisite for the development of silicon photonic chips. Regarding there is huge mode mismatching between them, it is very challenging to improve the coupling efficiency. Currently there are two kinds of popular approaches. One is using waveguide grating couplers, and the other one is using inversed taper couplers. The approach of using grating couplers enables wafer-scale testing with vertical fiber probes, in which way the alignment tolerance is relatively large. For conventional 1D grating couplers, however, the coupling efficiency and the 1-dB-bandwidth are still quite limited. Furthermore, grating couplers are usually strongly polarization-selective due to the birefringence of SOI strip waveguides. In order to solve these issues, some improved designs have been proposed [142–170]. For example, SWG-assisted grating couplers have been introduced [150], in which case a new degree of freedom is provided for the design. A comprehensive review was given in details in [150] for

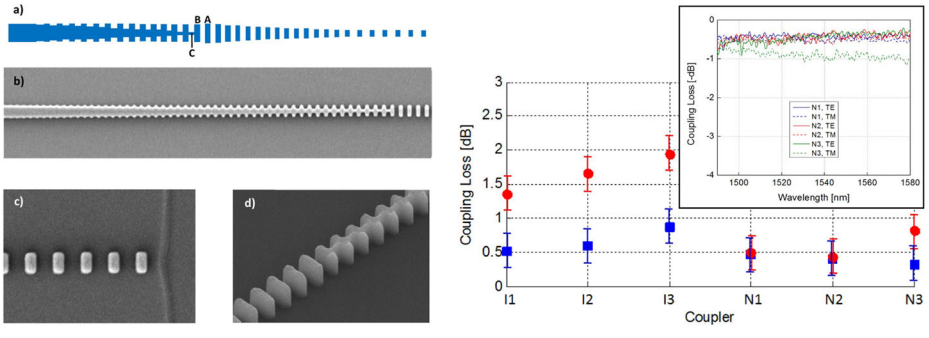

Fig. 8 a An SWG-assisted inversed taper for efficient fiber-chip couplings; **b** An SWG taper introduced to connect an SOI strip waveguide and an SWG waveguide; **c** Measured fiber-chip coupling loss [173]

various advanced grating couplers for achieving broad bandwidths, polarization insensitivity, perfect vertical-coupling, etc.

As an alternative approach, the edge coupling based on an inversed taper coupler is also very popular. For the inversed taper, the waveguide is adiabatically narrowed down to be e.g. less than 100 nm at the facet connected to the singlemode fiber. In this way, the mode field diameter at the facet is expanded accordingly and becomes matched well to that of a singlemode fiber. On the other hand, the fabrication is not easy regarding the tiny tip (<100 nm). Fortunately, the requirement for the fabrication can be relaxed with the help of SWG structures [171–173], as shown in Fig. 8(a). When SWG structures are introduced, the refractive-index contrast for the equivalent optical waveguide can be modified possibly by simply varying the duty-circle of the SWG structure (without any other materials introduced). An SWG taper can be introduced to connect a conventional SOI strip waveguide and an SWG waveguide, as shown in Fig. 8(b). With SWG-assisted inversed taper, the polarization dependence is negligible and a low coupling loss of <0.4 dB was achieved for the wavelength-band around 1550 nm [173], as shown in Fig. 8(c). For this design, the minimal feature size is 100 nm, for which the fabrication is not difficult for modern nanofabrication technologies. Therefore, this provides a promising option for efficient and broadband fiber-chip coupling.

Subwavelength silicon photonics for higher-order-mode manipulation

Recently, some emerging applications with higher-order modes makes multimode silicon photonics more and more popular. As a result, it is very desired to develop various high-performance multimode photonic devices on silicon for the manipulation of higher-order modes. Currently many multimode silicon photonic devices have been developed, e.g., on-chip mode (de) multiplexers [174–193], higher-order mode generator and exchanger [194–214], multimode splitter [215–220], MWBs [221–236], MWCs [237–251], etc. In this section, we give a review to show how SWG structures help the realization of silicon photonic devices and circuits for the manipulation of higher-order modes, including mode-selective couplers, multimode add-drop multiplexers, MWBs and MWCs.

Subwavelength silicon photonics for higher-order mode coupling/conversion

SWG-assisted mode-selective couplers

Mode-selective couplers are very important for multimode (de) multiplexing and multimode add-drop multiplexing in multimode photonics. In the past years, various mode-selective couplers have been developed by using different structures, e.g., multimode interferometers [175], asymmetric Y-junctions [176, 177], topology structures [178], adiabatic tapers [179, 182], ADCs [183–185], grating-assisted couplers [186], etc. As summarized in the previous review paper [22], these devices can be divided into three categories in principle. The first one is using the multimode interference in multimode sections, the second one is using the mode evolution in an adiabatic structure, and the third one is using cascaded ADCs consisting of two non-identical waveguides in the coupling region. Currently the latter two are more popular for realizing multi-channel

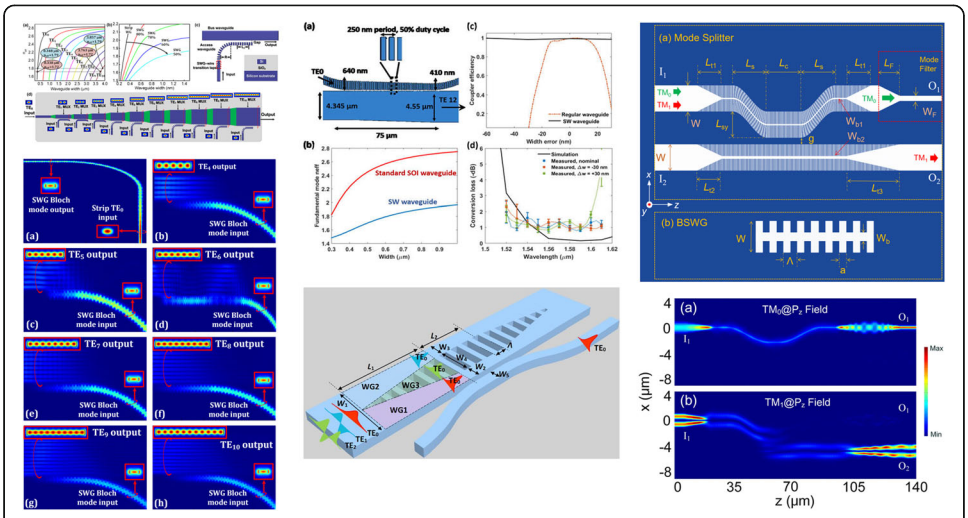

Fig. 9 a A 12-channel mode (de) multiplexer based on SWG-assisted ADCs [187]; **b** Higher-order mode (de) multiplexer based on an SWG-assisted dual-core adiabatic tapers [190]; **c** An SWG-assisted multimode add-drop multiplexer [191]; **d** Mode (de) multiplexer based on bridged SWG waveguides [193]

mode (de) multiplexers because of flexible structural design, high scalability, and excellent performances.

For example, in the past years high-performance mode (de) multiplexers with three- [180] and four- [181] channels were demonstrated for TE-polarization modes by using adiabatic dual-core tapers in cascade. Later, a broadband 10-channel mode (de) multiplexer with dual polarizations was realized with cascaded dual-core adiabatic tapers and PBSs for the first time [174]. A 12-channel mode (de) multiplexer for TE-polarization modes was demonstrated with SWG-assisted ADCs in cascade [187], as shown in Fig. 9(a). In this design, the SWG access waveguide is optimized to improve the fabrication tolerance. For the fabricated devices, the measured insertion losses ranging from 0.1 dB ~ 2.6 dB, and the crosstalk values ranging from −15.4 dB to −26.4 dB are obtained at 1545 nm, for all the 11 channels. In the wavelength range of 1520 nm to 1570 nm, the overall insertion losses are lower than 5.2 dB, and the crosstalk values are below −10.0 dB More recently, in [190] a mode-selective coupler for the 12th higher-order mode was demonstrated by using an SWG-assisted adiabatic coupler, as shown in Fig. 9(b). Here the SWG waveguide was also used to improve the fabrication tolerance because the sensitivity of the effective index to the core-width variation is reduced. With this design, the mode-selective coupling efficiency is better than −1.5 dB over a 75-nm bandwidth and tolerates a fabrication variation of ±30 nm.

In order to selectively add/drop any mode-channel from the bus waveguide, it is desired to develop a multimode add-drop multiplexer. This device is different from those multi-channel mode (de) multiplexers, in which the bus waveguide is usually tapered and does not supporting all the mode-channels any more. Recently, a multimode add-drop multiplexer was proposed for the first time by utilizing the mode evolution assisted with SWG structures, as shown in Fig. 9(c). In this example, the multimode bus waveguide supporting three mode-channels for MDM systems is considered [191]. In particular, there is an SWG-assisted mode evolution region inserted in the multimode bus waveguide, so that the TE_0, TE_1 and TE_2 modes can be finally localized in

the left, middle, and right regions, respectively. With this design, one can add/drop any mode-channel by placing a singlemode access waveguide at the left or right side of the bus waveguide. Basically speaking, the width of the singlemode access waveguide should be chosen optimally according to the phase-matching condition. The field localization in the bus waveguide helps a lot to enhance the mode-selective coupling and thus high ERs can be achieved even for the fundamental mode in the bus waveguide (which is very difficult in conventional ADCs). In this way, a multimode add-drop multiplexer is realized to add-to/drop-from a multimode bus waveguide not only for higher-order modes but also for the fundamental mode.

Most recently, a broadband mode-selective coupler is introduced to separate the TM_0 and TM_1 mode by the phase controlling of the bridged SWG waveguides [see Fig. 9(d)] [193]. Here the TM_0 mode is influenced by the central bridge much more than the TM_1 mode. Therefore, such a DC can be regarded as an asymmetric and symmetrical DC for the TM_0 and TM_1 modes, respectively. As a result, the TM_1 mode is expected to be cross-coupled, while the TM_0 mode has no crossing-coupling almost due to the high phase-mismatching. In this way, the TM_0 and TM_1 modes ae separated. The fabrication tolerances were also investigated, for the fabrication error of ± 20 nm, the deteriorations of the insertion loss and CT were less than 0.26 dB (1.47 dB) and 3.7 dB (9.8 dB) for the TM_0 mode (TM_1 mode), respectively. The fabrication error has greater influence on the TM_1 mode because the phase-matching condition is required.

SWG-assisted higher-order mode generators/exchangers

Higher-order mode converters are key fundamental elements for realizing higher-order mode generation as well as mode-exchange in multimode photonic systems. Previously on-chip higher-order mode converters were usually designed with a complicated structure consisting of a mode splitter, a mode interferometer and a mode combiner [194, 195]. It is also possible to realize mode converters by using cascaded tapered waveguides [196], which however is long (e.g., 13-23 μm). More recently, very compact $TE_{0\text{-}1}$ mode converters have been proposed and designed to generate the TE_1 mode from the TE_0 mode by utilizing the topology optimization [197–203]. For these mode converters, the footprints are usually very compact (e.g., 1.4×3.4 μm^2 [203]). However,

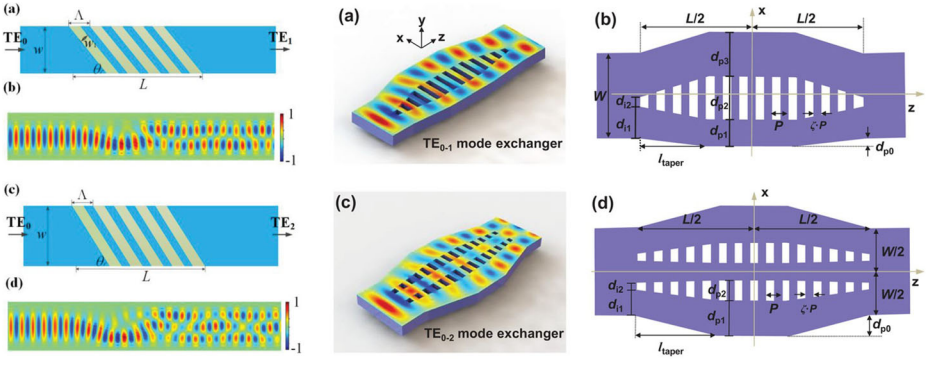

Fig. 10 a An on-chip mode-converter [213]; **b** An on-chip mode-exchanger [214]

the EL is as high as ~2 dB and the ER is ~9.5 dB within a bandwidth of 100 nm even in theory [203]. In [204], the $TE_{0\text{-}1}$ mode exchanger designed inversely has an EL of 1.0-2.2 dB and an ER is 9.3-10.6 dB for the 1525-1565 nm range in experiments. Furthermore, there are some irregular structures introduced with very tiny feature sizes (e.g., < 80 nm [199, 203]), which increases the fabrication difficulty. As an alternative, metamaterial or metasurface waveguides have been utilized for realizing on-chip higher-order mode converters [205–213].

For the mode exchanger based on shallowly-etched dielectric metasurface waveguide in [205], the device is 23-μm-long and the EL is about 0.8 dB. Moreover, tilting the grating elements provide a new method to control the anisotropy of the metamaterial. As shown in ref. [207], a 45°-tilted grating introduces an effective index variation of 0.23 for the TE_0 mode, whereas the change for the TM modes is 20 times smaller. Recently an ultra-compact mode converter was proposed and demonstrated with a metasurface structure with a tilted subwavelength periodic perturbation [213], as shown in Fig. 10(a). For the TE_{01} and TE_{02} mode converters, which are respectively for realizing the conversion from the TE_0 mode to the TE_1 and TE_2 modes, the lengths are about 6 μm, the conversion losses are <1 dB and the ERs are >10 dB. It is still challenging to achieve compact high-performance higher-order-mode converters with very low ELs and high ERs in an ultra-broad wavelength-band. Recently a novel concept of realizing on-chip higher-mode generation/exchange was proposed by using metamaterial structures where multimode excitations and multimode interferences are manipulated carefully [214], as shown in Fig. 10(b). The demonstrated $TE_{i\text{-}j}$ mode exchangers are very compact and enable efficient exchange between the TE_i and TE_j modes. For the demonstrated $TE_{0\text{-}1}$ and $TE_{0\text{-}2}$ mode exchangers, the footprints are respectively as compact as 1.3×2.7 μm^2 and 1.9×2.9 μm^2, while the ELs are as low as 0.19-0.45 dB and the ERs are >10 dB in ultrabroad bandwidths up to 350-400 nm, which are the best ones reported to date.

Dual-mode 2×2 3dB power splitters

As mentioned above, a 2×2 3dB power splitter is a fundamental element for many photonic systems. However, for the case with higher-order modes, the situation becomes very different and there is very few result reporting 2×2 3dB power splitters with multiple mode-channels. Recently, a dual-mode 3dB power coupler was realized by utilizing

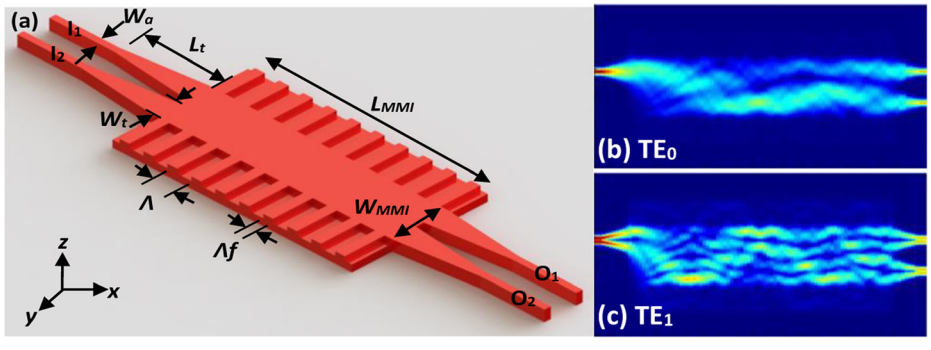

Fig. 11 Dual-mode 2×2 3dB power splitter [220]

a tapered waveguide [215], a Y-branch [216, 217], and an inverse design [218, 219]. Unfortunately, the bandwidth is still quite limited and the footprint is large. Currently, it is still a big challenge to achieve high-performance multimode 2×2 3dB power splitter. More recently, a dual-mode 2×2 3dB power splitter was proposed and demonstrated by using an MMI coupler with shallowly-etched SWG structures [220], as shown in Fig. 11(a)-(c). In particular, the shallowly-etched SWG structure is used to spatially modify the refractive index profile of the MMI section in the lateral direction. In this way, the phase errors of the guided-modes excited in the MMI section can be minimized. As a result, a high-performance MMI coupler with a low EL and imbalance (IB) is achieved for both input modes when the phase error of the higher-order modes in the MMI region is reduced through engineering the refractive index profile. For the designed device, the ELs are <0.32 dB and < 0.8 dB while the IB is < 0.1 dB and < 0.3 dB in the wavelength range of 1.52-1.58 μm for the incident TE_0 and TE_1 modes, respectively.

Subwavelength silicon photonics for higher-order mode propagation

SWG-assisted multimode waveguide bends (MWBs)

Waveguide bends are usually inevitable for building PICs and previously lots of works were focusing on sharp bends for singlemode waveguides [221–225]. For multimode photonics, sharp multimode waveguide bends (MWBs) are extremely important. However, there is strong modal field distortion in a sharp MWB and thus significant mode mismatch might happen at the straight-bent junction [226], which introduces significant mode-mismatching loss as well as inter-mode crosstalk [226–236]. Currently there are mainly three approaches for achieving sharp MWBs. The first one is using a special bent section whose curvature varies from zero to a given value gradually, so that the guided modes in the bent section can be converted gradually with negligible mode distortion [229, 230]. With this approach, one can realize very broadband MWBs with low

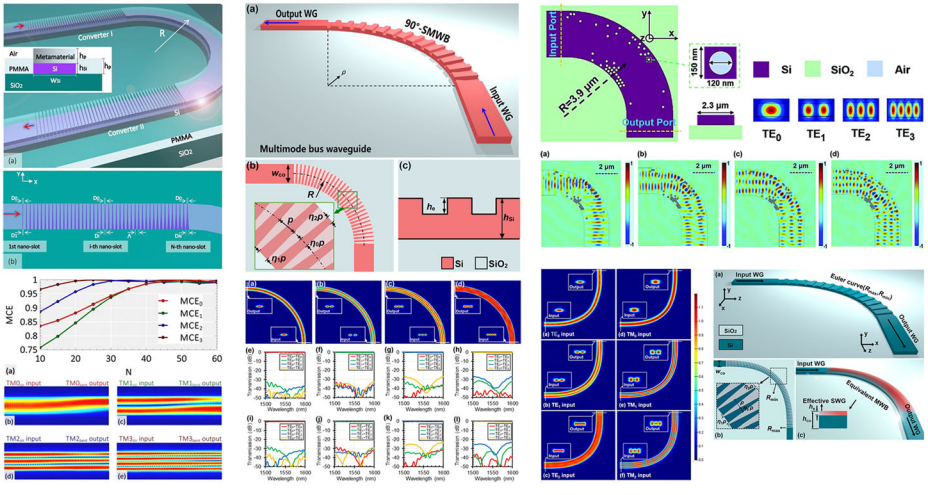

Fig. 12 **a** A sharp MWB with mode converters based on a metamaterial-assisted PMMA upper-cladding [233]; **b** A 90°-MWB based on shallowly-etched non-uniform SWGs [237]; **c** A sharp MWB based on a pixelated meta-structure [238]; **d** A sharp MWB for six dual-polarization modes realized by combining the designs with modified Euler-curve and shallowly-etched non-uniform SWGs [239]

ELs, low inter-mode crosstalk and relatively large effective bending radius (e.g., several tens of microns).

The second one is to introduce some special mode converter between the straight and bent sections, so that the guided-modes launched from the straight section could be converted to the guided-modes in the bent section [231–234]. For example, in [233] a multimode converter with a SWG-assisted polymethyl methacrylate (PMMA) upper-cladding was introduced for realizing sharp MWBs, as shown in Fig. 12(a). For the demonstrated with 90° MWB, the arc-bend radius is R=30 μm. Meanwhile, the length of the mode converter is L_{tp}=15.8 μm, which is required to be long enough for adiabaticity. In this case, the effective radius for the demonstrated MWB is given as R′=45.8 μm (i.e., R + L_{tp}). Correspondingly, this MWB works very well with low ELs less than 1 dB and low crosstalk less than −20 dB over an 80 nm wavelength band for four TM mode-channels, as shown in measured results.

The third one is modifying the refractive-index profile in the bent section, so that the mode-mismatch can be minimized [141, 238]. In [237], a sharp MWB was proposed and demonstrated by introducing shallowly-etched SWG structures in the bent section, as shown in Fig. 12(b). Here the SWG structure spatially modifies the effective-index profile in the bent section, in which way the equivalent refractive index profile of the bent section is matched very well with that of the straight multimode waveguide. As a result, one can minimize the mode mismatching between the bent and straight sections. For the realized MWB with an ultra-small bending radius of R=10 μm, the ELs are 0.5-0.8 dB and the inter-mode crosstalk is <−20 dB in a broad bandwidth for all three TE modes, which is one of the best results to date. Inverse design method utilizing pixelated meta-structure provided an alternative way to achieve an ultra-compact waveguide bend, as shown in Fig. 12(c). For the realized MWB with a small bending radius of R=3.9 μm, the measured ELs are <1.8 dB and the CTs are <−17 dB for the TE_0, TE_1, TE_2 and TE_3 modes in the wavelength band of 1530-1570 nm.

It is also possible to combine more than one method mentioned above together, so that the MWB performance could be improved. Recently, a special MWB was proposed by combing the designs with modified Euler-curve and shallowly-etched non-uniform

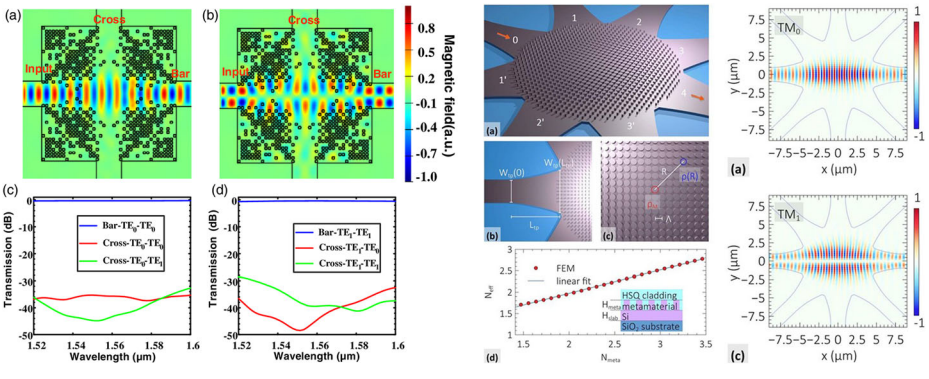

Fig. 13 a Dual-mode waveguide crossings based on a subwavelength-structured MMI coupler [248]; **b** A multi-port MWC using a metamaterial Maxwell's fisheye lens [251]

SWGs. Here the curvature of the SWG-assisted bent section varies from a near-zero value to a given value gradually, as shown in Fig. 12(d) [239]. In this way, an ultra-sharp MWB was presented to work with dual polarizations for the first time. For the designed 90°-MWB, which has a core width of 1.01 μm and an effective bending radius as small as 10 μm, the ELs are less than 0.23 dB and the inter-mode crosstalk is lower than <−26.5 dB over a broad band from 1500 nm to 1600 nm for six mode-channels, including three TE-polarization modes and three TM-polarization modes. This can be extended for more mode-channels, which provides a promising approach for realizing high-density multimode silicon photonics in the future. The designed MWB still work well with low inter-mode CT (e.g., <−20 dB) in the broad wavelength-band from 1500 nm to 1600 nm even when there are some fabrication errors for Δw = ±20 nm, Δh_e = ±10 nm and $\Delta \eta_1 \rho$ = ±20 nm.

Multimode waveguide crossings (MWCs)

Low-loss and low-crosstalk MWCs are also very important for large-scale multimode PICs (e.g., photonic networks-on-chip). Even though many smart designs are available for singlemode waveguide crossings [240–245], there are no much work on the development of MWCs, which is challenging because of the involvement of the higher-order modes. In the past years, several types of MWCs were realized by introducing some special structural designs [246–249]. For example, one can use multiple regular single-mode waveguide crossings by converting the higher-order modes to the fundamental one [246, 247]. It is also possible to use a special MMI section designed to simultaneously work for the fundamental and higher-order modes [248, 249].

As shown in Fig. 13(a), a dual-mode waveguide crossing based on a subwavelength-structured MMI coupler was proposed and demonstrated [248]. In this design, the footprint is as compact as 4.8×4.8 μm^2. For the fabricated dual-mode waveguide crossing, the ELs are as low as ~0.6 dB and the crosstalk are less than −24 dB in a broad bandwidth from 1530 nm to 1590 nm. In [251], a novel multi-port MWC was proposed and demonstrated for the first time by using a metamaterial-based Maxwell's fisheye lens. As shown in Fig. 13(b), this lens was realized by introducing silicon nano-rods with varied diameters. Any guided-mode launched at the end of the input port can be focused and imaged at the end of the output port and finally coupled to the corresponding guided mode in the output waveguide. For the fabricated eight-port MWC, the ELs are as low as ~0.3 dB and the crosstalk are less than −20 dB in a broad bandwidth from 1520 nm to 1600 nm. This multi-port MWC is very useful for complicated multimode PICs with many waveguide paths, and thus introduces high flexibility for the layout design of large-scale PICs in the future.

Emerging applications

There have been many applications by utilizing unique mode manipulation in subwavelength silicon photonics based on SSWGs and HPWGs. In particular, silicon HPWGs with ultra-strong field enhancement in the low-index nano-slot region has low propagation losses of ~0.01 dB/μm. Furthermore, the SOI-compatibility of silicon HPWGs paves the way to seamlessly merge SOI strip waveguides for long-distance mode propagation and HPWGs for local mode manipulation. In this way, on-chip photonic devices

assisted locally by HPWGs can have acceptably low losses and ultra-compact footprints, which are attractive for the development of integrated photonics [6–10]. For silicon SSWGs, there are also lots of opportunities to effectively manipulate the guided-mode properties, including the effective indices, the mode fields, the birefringence, and the mode dispersion. More importantly, SSWGs usually have low propagation losses of about 2 dB/cm [11–13], which is similar to the loss of regular strip waveguides. Therefore, SSWGs have attracted intensive attention in the development of photonic devices for many emerging applications in recent years, including wavelength-selective photonic devices, enhancement of light-matter interaction, dispersion-engineering, two-beam interferometers, as described below.

Wavelength-selective photonic devices with subwavelength mode-manipulation

Wavelength-selective photonic devices have been recognized as key elements in optical communications and microwave photonic systems [252]. Among various wavelength-selective structures, Bragg gratings with a periodic variation of effective-index along the direction of light propagation have been used very popularly. As it might be noticed, the high index-contrast of silicon photonic waveguides hinders the realization of narrow-band Bragg-grating filters, which often requires the corrugation widths of a few nanometers or double-etch geometries. Since the effective index of SWG waveguides could be manipulated flexibly, a novel Bragg grating can be formed by interleaving two SWG waveguides with different duty cycles, as demonstrated in [253]. The demonstrated SWG Bragg grating has a peak reflectivity of about >90% and exhibits a 3 dB bandwidth of 0.5 nm. It can be seen the SWG structure provides an interesting flexibility of device designs. Another SOI Bragg filters based on sub-wavelength index engineering in a differential corrugation width configuration, as demonstrated in [254]. Such a double-periodicity structure enables narrow-band notch filtering with a single etching-step and relaxed width constraints. The demonstrated SWG Bragg-grating filter with minimum transversal and longitudinal features of 150 nm and 85 nm shows a rejection bandwidth of 1.1 nm and an extinction ratio exceeding 40 dB. Such a photonic filter is useful for pump-rejection filtering in the realization of on-chip quantum photon-pair sources.

Add-drop photonic filters [255, 256] could also be achieved with subwavelength mode-manipulation in Bragg gratings. For example, in [255] an ultra-broadband add-drop photonic filter was realized by inserting two identical SWG waveguides into the MZI arms. In particular, the SWG waveguides were designed with a band-edge wavelength of ~1565nm, so that the filter exhibits a high extinction ratio of >35 dB and a nearly flat-top band exceeding 40 nm for both stopband and passband. High-performance multi-channel photonic filters could also be achieved by cascading more than one contra-DCs consisting of a Bragg-grating bus waveguide and a SWG waveguide, as shown in [256]. Here the contra-DCs are short because the evanescent coupling is strong due to the weakened optical confinement of the used SWG waveguides.

As a summary, it is possible to have more and more opportunities for realizing novel special wavelength-selective photonic devices with the help of subwavelength mode-manipulation.

Enhancement of light-matter interaction with subwavelength mode-manipulation

Enhancement of light-matter interaction is the fundamental key for many applications, such as optical sensing, optical modulation, optical forcing, etc. There are lots of work reported in recent years. Basically, it is very useful by introducing some special subwavelength waveguides with field enhancement, such as the silicon HPWGs and SWG waveguides considered in the present paper. In recent years, SWG waveguides have been recognized to be useful for optical-force manipulation, providing an interesting approach for on-chip nano-particle trapping. As analyzed in [257], an SWG waveguide can trap many nano-particles stably periodically, which is very different from the case with a conventional strip optical waveguide and thus is useful for the applications of multi-particle manipulating.

SWG structures have also been introduced to micro-cavities for the realization of high-sensitivity optical sensors [258–260]. Compared to conventional strip waveguides, SWG waveguides have better sensitivity and lower detection limit because of the enhanced photon-analyte interaction. As demonstrated in [258–260], an SWG microresonator on silicon was presented with a relatively low Q-factor of 7000~9800, showing a bulk sensitivity of 430~490 nm/RIU (refractive index unit) and a detection limit of 3.7×10^{-4}~2×10^{-6} RIU. More recently, a silicon SWG microdisk sensor for mid-infrared was also proposed and demonstrated with a high sensitivity. In particular, the bending radius is chosen as small as 6 μm and a free spectral range of 40.3 nm was obtained to enabling a large dynamic range of measurements. NaCl aqueous solution with a varied concentration was measured with a sensitivity of about 390.4 nm/RIU. For SWG micro-resonators, one should further reduce the bending loss as well as the scattering losses for SWGs by improving the structural design and the fabrication process.

Furthermore, high-efficiency optical modulators and optical switches could also be realized possibly by using SWG waveguides [261] with electro-optic (EO) materials as well as silicon HPWG with vanadium dioxide [262]. In [261], an SWG waveguide filled with EO-polymer was introduced for realizing high-speed optical modulators with a 3-dB-bandwidth of >40 GHz because the mode confinement factor of EO-polymer is as high as 36.2%, which is about nine times higher than that (~4.0%) for a typical SOI strip waveguide. In [262], an optical switch based on a silicon HPWG was proposed by utilizing the phase change properties of VO_2. The proposed switch shows an extinction ratio of 4.32 dB/μm and an insertion loss of 0.88 dB/μm. In this design, the field enhancement of the silicon HPWG and the significant change of the VO_2 refractive index make it possible to have a very compact modulation section as short as 3 μm.

As it can be seen, light-matter interaction can be effectively enhanced by using special subwavelength waveguides with field enhancement, which can help a lot for more emerging applications in the future.

Dispersion-engineering with subwavelength mode-manipulation

As it is well known, dispersion engineering plays an important role for realizing specific wavelength-dependence of photonic devices, including relief or enhancement of the wavelength dependence as desired. For example, dispersion-engineered structures have been developed with strong dispersion for realizing slow light, so that light-matter

interaction is significantly enhanced. This is very attractive for efficient optical modulators, compact tunable delay lines and high-sensitivity optical sensing.

For example, slow light can be achieved by engineering the SWG waveguide dispersion such that the band-edge is located within the desired wavelength-band, as demonstrated in [263]. The position of the band-edge can be shifted flexibly by varying the SWG period. And the bandwidth increases with the index contrast as well as the duty-cycle. The experiment results showed that a high group index of up to 47.7 was achieved with a loss lower than 1.5 dB/mm in a bandwidth as large as 8.8 nm. Similarly, in [264] slow light was demonstrated in SWG waveguides integrated on a silicon photonic chip, and the group index is up to 30 at the band-edge. Such slow-light SWG waveguides are useful for realizing compact tunable delaylines as well as enhancing the light-matter interaction in optical modulators and optical sensors.

SWG waveguides have also be used as optical delaylines with the required incremental time delay through precisely modifying the group index in the waveguide. In [265], an integrated index-variable optical true time delay line (OTTL) was demonstrated by using SWG waveguides with optimized duty-cycles, enabling the realization of OTTDLs with a simple geometry and a compact chip area. Furthermore, such an index-variable OTTDL has an extremely broad operation bandwidth exceeding several tens of THz, supporting the operation for various input optical signals in a broadband wavelength bandwidth.

Besides, highly-dispersive coupling in an SWG directional coupler was achieved for a racetrack resonator by engineering the SWG waveguide structure, as shown in [266]. In this way, a V-shape envelope of resonance spectrum is achieved, and the change of the upper-cladding refractive index can be measured by monitoring the movement of the spectrum envelope peak, which is helpful for optical sensing.

As demonstrated in these work, dispersion-engineering has been achieved by utilizing the mode-manipulation in subwavelength waveguides, and plays an important role in more and more emerging applications.

Phase-shifting for interferometers with subwavelength mode-manipulation

Optical interferometers with two-/multi-beam interference is one of the most fundamental photonic devices for many applications. Among them, MZIs are one of the most representative devices. The key for MZIs is the manipulation of the phase shifting between the two beams, which is flexible when subwavelength mode-manipulation is introduced. Therefore, high-performance phase-shifters are extensively important in integrated optics not only for telecom and datacom applications, but also for sensors and quantum computing.

For example, an MZI with the assistance of SWG waveguides have been demonstrated for all-optical switching [267–269]. When using an SWG waveguide in one arm and a conventional strip waveguide in the other one, an optical path imbalance was produced due to the difference of their effective indices. In this design, the optical-path imbalance was produced without any bends, facilitating a very compact footprint. Furthermore, an SWG waveguide usually has a propagation loss similar to the regular strip waveguide, ensuring a high interference contrast, which is important for many

applications. Since the optical power density in the SWG waveguide is ~15 times less than that in the strip waveguide, the nonlinear refractive-index change triggered inside the strip waveguide is much stronger than that in the SWG waveguide when the proper condition is met. As a result, a phase difference is introduced between the MZI arms. Accordingly, a novel ultra-fast all-optical MZI was realized for all-optical picosecond sampling and switching.

MZIs with SWGs were further used to be arrayed for producing a Fourier-transform spectrometer, as demonstrated in [270]. Here there are 32 MZIs with SWGs, for which the optical path difference was presented without waveguide bends. Furthermore, since SWG waveguides have similar propagation losses to conventional strip waveguides, the loss imbalance is minimized and the extinction ratio is −25~−30 dB is obtained. The demonstrated on-chip spectrometer has a decent performance with a spectral resolution of 50 pm and a free-spectral range of 0.78 nm.

Recently, ultra-broadband phase-shifters have been noticed as an important element to address the operational requirements for the next generation of photonic integrated circuits for many applications. In [271], a novel phase-shifter based on SWG waveguides was demonstrated with ultra-broad bandwidth by exploiting the anisotropy and dispersion engineering in SWG waveguides. It is predicted theoretically that the phase shift error is below ±1.7° over an unprecedented operation range of >400 nm (i.e., 1.35-1.75 μm) covering the E, S, C, L and U telecommunication bands. This phase-shifter has very nice fabrication tolerance of up to ±20 nm, showing greater robustness than conventional waveguides. The proposed subwavelength-engineered phase-shifter paves the way for novel photonic integrated devices with an ultra-broadband performance.

Conclusion and outlook

In this paper, we have given a review for recent progresses of subwavelength silicon photonics with SSWGs and HPWGs for on-chip mode-manipulation, including three major parts. The first part is focused on subwavelength silicon photonics for the fundamental mode, including on-chip polarization-handling devices for the polarization modes, and power couplers/splitters for the fundamental mode. In the second part, we have focused on subwavelength silicon photonics for higher-order-mode manipulation, including the coupling/conversion and propagation of higher-order modes (e.g., MWBs and MWCs). In the end, some emerging applications were discussed. It can be seen that the introduction of subwavelength photonic waveguides such as SSWGs and HPWGs is helpful for realizing high-performance silicon photonic devices.

As a summary, subwavelength silicon photonics for flexible mode-manipulation is becoming more and more important for various applications. In particularity, one can effectively manipulate the field profiles, the effective indices, the birefringence as well as the waveguide dispersion for the guided-modes in subwavelength photonic waveguides. As a result, it provides an effective approach to realize silicon photonic devices with compact footprints, low ELs, low crosstalk, high ERs, as well as ultra-broad bandwidths, etc. It is also of great significance to further explore the utilization of subwavelength silicon photonics to deal with not only the fundamental mode but also the higher-order modes.

More effort is still needed to improve the fabrication tolerance so that the fabrication complexity can be reduced. This is very important for further performance

improvement of subwavelength silicon photonic devices and for the realization of large-scale photonic integration. As it might be noticed, the fabrication for both HPWGs and SSWGs is more difficult than regular SOI strip waveguides due to the deep subwavelength feature size. It even more challenging for the fabrication of metal strips in HPWGs, and thus there are less experimental results for HPWGs than SSWGs. Nevertheless, subwavelength photonic waveguides are still very attractive and popular regarding their unique properties. Meanwhile, note that the nanofabrication technologies are becoming more and more mature, which enables precise fabrication for sub-100nm feature sizes and helps a lot for the development of high-performance subwavelength silicon photonic devices. Therefore, it is desired to explore more emerging applications of subwavelength silicon photonics with smart mode manipulation in the future, such as on-chip optical sensing systems, high-capacity optical interconnects, as well as on-chip photonic computing systems.

Acknowledgements
Not applicable

Authors' contributions
C.L. and D.D. wrote the manuscript. C.L., M.Z., Y.T., Y.S. and D.D. read and approved the final manuscript. D.D. supported and supervised the research and provided guidance to the review.

Funding
This work was supported by National Major Research and Development Program (No. 2018YFB2200200/2018YFB2200201), National Science Fund for Distinguished Young Scholars (61725503), National Natural Science Foundation of China (NSFC) (91950205, 61961146003), Zhejiang Provincial Natural Science Foundation (LZ18F050001, LD19F050001), and the Fundamental Research Funds for the Central Universities.

Availability of data and materials
The datasets and figures used and analyzed during the current study are available from the corresponding author on reasonable request.

Declarations

Competing interests
The authors declare that they have no competing interests.

Received: 22 March 2021 Accepted: 12 May 2021
Published online: 13 July 2021

References

1. Agrell E, et al. Roadmap of optical communications. J Opt. 2016;18(6):063002.
2. Tkach RW. Scaling optical communications for the next decade and beyond. Bell Labs Tech J. 2010;14:3–9.
3. Eldada L. Advances in ROADM technologies and subsystems. Photonics North. International Society for Optics and Photonic. 2005; 5970:597022-597022-10.
4. Dong P, et al. Silicon photonic devices and integrated circuits. Nanophotonics. 2014;3:215–28.
5. Liang D, Bowers JE. Recent progress in lasers on silicon. Nat Photonics. 2010;4(8):511.
6. Dai D, He S. A silicon-based hybrid plasmonic waveguide with a metal cap for a nano-scale light confinement. Opt Express. 2009;17(19):16646–53.
7. Guan X, Wu H, Dai D. Silicon hybrid nanoplasmonics for ultra-dense photonic integration. Front Optoelectronics. 2014; 7(3):300–19.
8. Dai D, Wu H, Zhang W. Utilization of field enhancement in plasmonic waveguides for subwavelength light-guiding, polarization handling, heating, and optical sensing. Materials. 2015;8(10):6772–91.
9. Dai D, et al. Silicon hybrid plasmonic submicron-donut resonator with pure dielectric access waveguides. Opt Express. 2011;19(24):23671–82.
10. Dai D, et al. Gain enhancement in a hybrid plasmonic nano-waveguide with a low-index or high-index gain medium. Opt Express. 2011;19(14):12925–36.
11. Cheben P, et al. Subwavelength integrated photonics. Nature. 2018;560(7720):565–72.
12. Wang J, Glesk I, Chen LR. Subwavelength grating devices in silicon photonics. Sci Bull. 2016;61(11):879–88.
13. Donzella V, et al. Sub-wavelength grating components for integrated optics applications on SOI chips. Opt Express. 2014;22(17):21037–50.
14. Bogaerts W, et al. A polarization-diversity wavelength duplexer circuit in silicon-on-insulator photonic wires. Opt Express. 2017;15(4):1567–78.
15. Barwicz T, et al. Polarization-transparent microphotonic devices in the strong confinement limit. Nat Photonics. 2007; 1(1):57–60.

16. Dai D, et al. Polarization management for silicon photonic integrated circuits. Laser Photonics Rev. 2013;7(3):303–28.
17. Fukuda H, et al. Silicon photonic circuit with polarization diversity. Opt Express. 2008;16(7):4872–80.
18. Pfau T, et al. Coherent digital polarization diversity receiver for real-time polarization-multiplexed QPSK transmission at 2. 8 Gb/s. IEEE Photon Technol Lett. 2007;19(24):1988–90.
19. Dong P, et al. Monolithic silicon photonic integrated circuits for compact 100Gb/s coherent optical receivers and transmitters. IEEE J Select Top Quantum Electron. 2014;20(4):150–7.
20. Feng L, et al. On-chip coherent conversion of photonic quantum entanglement between different degrees of freedom. Nat Commun. 2016;7(1):1–7.
21. Zhou Z, Bai B, Liu L. Silicon on-chip PDM and WDM technologies via plasmonics and subwavelength grating. IEEE J Select Top Quantum Electron. 2018;25(3):1–13.
22. Li C, Liu D, Dai D. Multimode silicon photonics. Nanophotonics. 2018;8(2):227–47.
23. Li C, et al. Silicon-based on-chip hybrid (de) multiplexers. SCIENCE CHINA Inf Sci. 2018;61(8):080407.
24. Xu H, Shi Y. On-chip silicon TE-pass polarizer based on asymmetrical directional couplers. IEEE Photon Technol Lett. 2017;29(11):861–4.
25. Dai D, Wang Z, Julian N, Bowers JE. Compact broadband polarizer based on shallowly-etched silicon-on-insulator ridge optical waveguides. Opt Express. 2010;18:27404–15.
26. Xiong Y, et al. High ER and broadband silicon TE-pass polarizer using subwavelength grating index engineering. IEEE Photonics J. 2015;7(5):1–7.
27. Chi J, et al. High-performance transverse magnetic mode-pass polarizer based on silicon nitride–silicon subwavelength grating waveguide for mid-infrared wavelengths. Appl Phys Express. 2018;11(4):042005.
28. Guan X, et al. Low-loss ultracompact transverse-magnetic-pass polarizer with a silicon subwavelength grating waveguide. Opt Lett. 2014;39(15):4514–7.
29. Ni B, Xiao J. Subwavelength-grating-based compact and broadband TE-pass polarizer for slot waveguides on a SOI platform. JOSA B. 2019;36(8):2126–33.
30. Zafar H, et al. Compact silicon TE-pass polarizer using adiabatically-bent fully-etched waveguides. Opt Express. 2018; 26(24):31850–60.
31. Xu H, Dai D, Shi Y. Anisotropic metamaterial-assisted all-silicon polarizer with 415-nm bandwidth. Photonics Res. 2019; 7(12):1432–9.
32. Bai B, et al. Low loss, compact TM-pass polarizer based on hybrid plasmonic grating. IEEE Photon Technol Lett. 2017; 29(7):607–10.
33. Abd-Elkader A, et al. Ultracompact AZO-based TE-pass and TM-pass hybrid plasmonic polarizers. JOSA B. 2019; 36(3):652–61.
34. Xu Z, Sun X. Ultra-broadband TE-pass polarizer based on hybrid plasmonic-assisted contra-directional couplers. JOSA B. 2020;37(2):251–6.
35. Zhang J, Cassan E, Zhang X. Wideband and compact TE-pass/TM-stop polarizer based on a hybrid plasmonic Bragg grating for silicon photonics. J Lightwave Technol. 2014;32(7):1383–6.
36. Azzam S, Obayya S. Ultra-compact resonant tunneling-based TE-pass and TM-pass polarizers for SOI platform. Opt Lett. 2015;40(6):1061–4.
37. Guan X, et al. Ultra-compact broadband TM-pass polarizer using a silicon hybrid plasmonic waveguide grating. In: Proceedings of Asia Communications and Photonics Conference. Beijing, 2013; ATh4A.
38. Guan X, et al. Ultra-compact and ultrabroadband TE-pass polarizer with a silicon hybrid plasmonic waveguide. In: Proceedings of SPIE Photonics West. San Francisco. 2014; 8988
39. Alam M, et al. Compact hybrid TM-pass polarizer for silicon-on-insulator platform. Appl Opt. 2011;50(15):2294–8.
40. Alam M, et al. Compact and silicon-on insulator-compatible hybrid plasmonic TE-pass polarizer. Opt Lett. 2012; 37(1):55–7.
41. Huang Y, et al. CMOS compatible horizontal nanoplasmonic slot waveguides TE-pass polarizer on silicon-on-insulator platform. Opt Express. 2013;21(10):12790–6.
42. Sun X, et al. Experimental demonstration of a hybrid plasmonic transverse electric pass polarizer for a silicon-on-insulator platform. Opt Lett. 2012;37(23):4814–6.
43. Ni B, Xiao J. Plasmonic-assisted TE-pass polarizer for silicon-based slot waveguides. IEEE Photon Technol Lett. 2018;30(5): 463–6.
44. Huang T. TE-pass polarizer based on epsilon-near-zero material embedded in a slot waveguide. IEEE Photon Technol Lett. 2016;28(20):2145–8.
45. Xu Y, Xiao J. A compact TE-pass polarizer for silicon-based slot waveguides. IEEE Photon Technol Lett. 2015; 27(19):2071–4.
46. Azzam S, et al. Proposal of an ultracompact CMOS-compatible TE-/TM-pass polarizer based on SOI platform. IEEE Photon TechnolLett. 2014;26(16):1633–6.
47. Ni B, Xiao J. A compact silicon-based TE-pass polarizer using three-guide directional couplers. IEEE Photon Technol Lett. 2017;29(19):1631–4.
48. Sun X, Mojahedi M, Aitchison J. Hybrid plasmonic waveguide based ultra-low insertion loss transverse electric-pass polarizer. Opt Lett. 2016;41:4020–3.
49. Azzam S, Obayya S. Titanium nitride-based CMOS compatible TE-pass and TM-pass plasmonic polarizers. IEEE Photon Technol Lett. 2016;28(3):367–70.
50. Alam M, Aitchison J, Mojahedi M. Compact and siliconon-insulator-compatible hybrid plasmonic TE-pass polarizer. Opt Lett. 2012;37:55–7.
51. Hameed M, Zaghloul R, Azzam S, Obayya S. Ultrashort hybrid plasmonic transverse electric pass polarizer for siliconon-insulator platform. Opt Eng. 2017;56:017107.
52. Ying Z, et al. Ultracompact TE-pass polarizer based on a hybrid plasmonic waveguide. IEEE Photon Technol Lett. 2015; 27(2):201–4.
53. Ng T, Khan M, Al-Jabr A, Ooi B. Analysis of CMOS compatible Cu-based TM-pass optical polarizer. IEEE Photon Technol Lett. 2012;24(9):724–6.

54. Xu Y, Xiao J. Design and numerical study of a compact, broadband and low-loss TE-pass polarizer using transparent conducting oxides. Opt Express. 2016;24:15373–82.
55. Lu Z, et al. Wideband silicon photonic polarization beam splitter based on point-symmetric cascaded broadband couplers. Opt Express. 2015;23(23):29413–22.
56. Dai D, Bowers J. Novel ultra-short and ultra-broadband polarization beam splitter based on a bent directional coupler. Opt Express. 2011;19(19):18614–20.
57. Wang J, et al. Realization of an ultra-short silicon polarization beam splitter with an asymmetrical bent directional coupler. Opt Lett. 2013;38(1):4–6.
58. Chen S, Wu H, Dai D. High extinction-ratio compact polarization beam splitter on silicon. Electron Lett. 2016;52(12): 1043–5.
59. Hsu C, et al. 8.13 μm in length and CMOS compatible polarization beam splitter based on an asymmetrical directional coupler. Appl Opt. 2016;55(12):3313–8.
60. Wu H. and Dai D. Novel high-performance polarization beam splitter on silicon. Asia Communications and Photonics Conference (ACP). 2016; IEEE.
61. Wu H, Tan Y, Dai D. Ultra-broadband high-performance polarizing beam splitter on silicon. Opt Express. 2017;25(6): 6069–75.
62. Wang X, et al. Ultra-small and fabrication-tolerant silicon polarization beam splitter using sharp bent directional coupler. IEEE Photonics J. 2018;10(5):1–7.
63. Huang T, et al. A slot-waveguide-based polarization beam splitter assisted by epsilon-near-zero material. Photonics Nanostructures Fundam Appl. 2019;33:42–7.
64. Fu P, et al. Optimization for ultrabroadband polarization beam splitters using a genetic algorithm. IEEE Photonics J. 2018;11(1):1–11.
65. Li C, Dai D. Compact polarization beam splitter for silicon photonic integrated circuits with a 340-nm-thick silicon core layer. Opt Lett. 2017;42(21):4243–6.
66. Chia-Chien H. Numerical investigations of an ultra-compact polarization beam splitter based on augmented low-index guiding and subwavelength grating structures. Sci Rep. 2018;8(1):1–11.
67. Bai B, Yang F, Zhou Z. Demonstration of an on-chip TE-pass polarizer using a silicon hybrid plasmonic grating. Photonics Res. 2019;7(3):289–93.
68. Zhang F, et al. Ultra-broadband and compact polarizing beam splitter in silicon photonics. OSA Continuum. 2020;3(3): 560–7.
69. Xie Y, et al. Combination of surface plasmon polaritons and subwavelength grating for polarization beam splitting. Plasmonics. 2020;15(1):235–41.
70. Xu Z, Lyu T, Sun X. Interleaved subwavelength gratings strip waveguide-based TM pass polarizer on SOI platform. IEEE Photonics J. 2020;12(2):4900110.
71. Chen Y, Xiao J. Compact silicon-based polarization beam splitter using directional couplers assisted with subwavelength gratings. Opt Eng. 2020;59(1):017101.
72. Xie Y, et al. Bloch supermode interaction for high-performance polarization beam splitting. Opt Eng. 2019;58(9):095102.
73. Shen B, et al. An integrated-nanophotonics polarization beamsplitter with 2.4× 2.4 μm^2 footprint. Nat Photonics. 2015; 9(6):378–82.
74. Xu L, et al. Compact broadband polarization beam splitter based on multimode interference coupler with internal photonic crystal for the SOI platform. J Lightwave Technol. 2019;37(4):1231–40.
75. Li C, Zhang M, Bowers JE, Dai D. Ultra-broadband polarization beam splitter with silicon subwavelength-grating waveguides. Opt Lett. 2020;45(8):2259–62.
76. Kim Y, et al. High-extinction-ratio directional-coupler-type polarization beam splitter with a bridged silicon wire waveguide. Opt Lett. 2018;43(14):3241–4.
77. Tian Y, et al. Compact polarization beam splitter with a high ER over S+ C+ L band. Opt Express. 2019;27(2):999–1009.
78. Huang Y, et al. Polarization beam splitter based on cascaded step-size multimode interference coupler. Opt Eng. 2013; 52(7):077103.
79. Zhang Y, et al. High-extinction-ratio silicon polarization beam splitter with tolerance to waveguide width and coupling length variations. Opt Express. 2016;24(6):6586–93.
80. Hu T, et al. A compact ultrabroadband polarization beam splitter utilizing a hybrid plasmonic Y-branch. IEEE Photonics J. 2016;8(4):1–9.
81. Xu Y, et al. Compact and high ER polarization beam splitter using subwavelength grating couplers. Opt Lett. 2016;41(4): 773–6.
82. Liu L, Deng Q, Zhou Z. Manipulation of beat length and wavelength dependence of a polarization beam splitter using a subwavelength grating. Opt Lett. 2016;41(21):5126–9.
83. Xu H, Dai D, Shi Y. Ultra-broadband and ultra-compact on-chip silicon polarization beam splitter by using hetero-anisotropic metamaterials. Laser Photonics Rev. 2019;13(4):1800349.
84. Xu D, et al. Silicon photonic integration platform—Have we found the sweet spot? IEEE J Select Top Quantum Electron. 2014;20(4):189–205.
85. Keyvaninia S, et al. Demonstration of a heterogeneously integrated III-V/SOI single wavelength tunable laser. Opt Express. 2013;21(3):3784–92.
86. Xiao X, et al. High-speed, low-loss silicon Mach–Zehnder modulators with doping optimization. Opt Express. 2013;21(4): 4116–25.
87. Lou F, Dai D, Wosinski L. Ultracompact polarization beam splitter based on a dielectric-hybrid plasmonic-dielectric coupler. Opt Lett. 2012;37(16):3372–4.
88. Guan X, et al. Ultracompact and broadband polarization beam splitter utilizing the evanescent coupling between a hybrid plasmonic waveguide and a silicon nanowire. Opt Lett. 2013;38(16):3005–8.
89. Guan X, et al. Extremely small polarization beam splitter based on a multimode interference coupler with a silicon hybrid plasmonic waveguide. Opt Lett. 2014;3(2):259–62.

90. Wu H, Guan X, and Dai D. Novel silicon polarization beam splitter with a horizontal hybrid nanoplasmonic waveguide. Asia Communications and Photonics Conference. Optical Society of America, 2014.
91. Dai D, Wu H. Realization of a compact polarization splitter-rotator on silicon. Opt Lett. 2016;41(10):2346–9.
92. Xu H, Shi Y. Ultra-compact and highly efficient polarization rotator utilizing multi-mode waveguides. Opt Lett. 2017; 42(4):771–4.
93. Liu L, Ding Y, Yvind K, Hvam J. Silicon-on-insulator polarization splitting and rotating device for polarization diversity circuits. Opt Express. 2011;19(13):12646–51.
94. Ding Y, Liu L, Peucheret C, Ou H. Fabrication tolerant polarization splitter and rotator based on a tapered directional coupler. Opt Express. 2012;20(18):20021–7.
95. Xu Y, Xiao J. Ultracompact and high efficient silicon-based polarization splitter-rotator using a partially etched subwavelength grating coupler. Sci Rep. 2016;6(1):27949.
96. Xu Y, Xiao J. Design of a compact and integrated TM-rotated/TE-through polarization beam splitter for silicon-based slot waveguides. Appl Opt. 2016;55(3):611–8.
97. Tan K, Huang Y, Lo G-Q, Lee C, Yu C. Compact highly-efficient polarization splitter and rotator based on 90° bends. Opt Express. 2016;24(13):14506–12.
98. Xiong Y, Xu D, Schmid J, Cheben P, Janz S, Ye W. Fabrication tolerant and broadband polarization splitter and rotator based on a taper-etched directional coupler. Opt Express. 2014;22(14):17458–65.
99. Wang Z, Dai D. Ultrasmall Si-nanowire-based polarization rotator. J Opt Soc Am B. 2008;25(5):747.
100. Aamer M, Gutierrez A, Brimont A, Vermeulen D, Roelkens G, Fedeli J, et al. CMOS compatible silicon-on-insulator polarization rotator based on symmetry breaking of the waveguide cross section. IEEE Photon Technol Lett. 2012;24(22):2031–4.
101. Chen L, Doerr C, Chen Y. Compact polarization rotator on silicon for polarization-diversified circuits. Opt Lett. 2011;36(4): 469–71.
102. Xu H, Shi Y. Subwavelength-grating-assisted silicon polarization rotator covering all optical communication bands. Opt Express. 2019;27(4):5588–97.
103. Wang Y, et al. Ultra-compact sub-wavelength grating polarization splitter-rotator for silicon-on-insulator platform. IEEE Photonics J. 2016;8(6):1–9.
104. Dai D, Tang Y, Bowers J. E. Mode conversion in tapered submicron silicon ridge optical waveguides. Opt Express. 2012; 20(12):13425–39.
105. Xiong Y, et al. Polarization splitter and rotator with subwavelength grating for enhanced fabrication tolerance. Opt Lett. 2014;39(24):6931–4.
106. Ma M, et al. Sub-wavelength grating-assisted polarization splitter-rotators for silicon-on-insulator platforms. Opt Express. 2019;27(13):17581–91.
107. Yin Y, Li Z, Dai D. Ultra-broadband polarization splitter-rotator based on the mode evolution in a dual-core adiabatic taper. J Lightwave Technol. 2017;35(11):2227–33.
108. Sacher W, et al. Polarization rotator-splitters in standard active silicon photonics platforms. Opt Express. 2014;22(4):3777–86.
109. Dai D. Advanced passive silicon photonic devices with asymmetric waveguide structures. Proc IEEE. 2018;106(12):2117–43.
110. Chang W, et al. Inverse design and demonstration of ultracompact silicon polarization rotator. 2019 Optical fiber communications conference and exhibition (OFC). IEEE, 2019.
111. Hu T, et al. A polarization splitter and rotator based on a partially etched grating-assisted coupler. IEEE Photon Technol Lett. 2016;28(8):911–4.
112. Liu L, Deng Q, Zhou Z. Subwavelength-grating-assisted broadband polarization-independent directional coupler. Opt Lett. 2016;41(7):1648–51.
113. Velasco, et al. Ultracompact polarization converter with a dual subwavelength trench built in a silicon-on-insulator waveguide. Opt Lett. 2012;37(3):365–7.
114. Gao L, et al. On-chip plasmonic waveguide optical waveplate. Sci Rep. 2015;5(1):1–6.
115. Xie A, et al. Efficient silicon polarization rotator based on mode-hybridization in a double-stair waveguide. Opt Express. 2015;23(4):3960–70.
116. Sangsik K, Qi M. Mode-evolution-based polarization rotation and coupling between silicon and hybrid plasmonic waveguides. Sci Rep. 2015;5:18378.
117. Bai B, Liu L, Zhou Z. Ultracompact, high ER polarization beam splitter-rotator based on hybrid plasmonic-dielectric directional coupling. Opt Lett. 2017;42(22):4752–5.
118. Xiong Y, et al. Robust silicon waveguide polarization rotator with an amorphous silicon overlayer. IEEE Photonics J. 2014; 6(2):1–8.
119. Chang Y, Yu T. Photonic-quasi-TE-to-hybrid-plasmonic-TM polarization mode converter. J Lightwave Technol. 2015; 33(20):4261–7.
120. Caspers J, et al. Experimental demonstration of an integrated hybrid plasmonic polarization rotator. Opt Lett. 2013; 38(20):4054–7.
121. Komatsu M, Saitoh K, and Koshiba M. Design of ultra-small mode-evolution type polarization rotator based on surface plasmon polariton. Integrated Photonics Research, Silicon and Nanophotonics. Optical Society of America, 2012.
122. Chen S, Shi Y, He S, Dai D. Low-loss and broadband 2 x 2 silicon thermo-optic Mach-Zehnder switch with bent directional couplers. Opt Lett. 2016;41(4):836–9.
123. Kwong D, Hosseini A, Zhang Y, Chen R. 1 × 12 unequally spaced waveguide array for actively tuned optical phased array on a silicon nanomembrane. Appl Phys Lett. 2011;99(5):051104.
124. Chen S, Shi Y, He S, Dai D. Compact eight-channel thermally reconfigurable optical add/drop multiplexers on silicon. IEEE Photon Technol Lett. 2016;28(17):1874–7.
125. He M, et al. High-performance hybrid silicon and lithium niobate Mach–Zehnder modulators for 100 Gbit s−1 and beyond. Nat Photonics. 2019;13(5):359–64.
126. Yamada H, Tao C, Ishida S, Arakawa Y. Optical directional coupler based on Si-wire waveguides. IEEE Photon Technol Lett. 2005;17(3):585–7.
127. Soldano L, Pennings E. Optical multi-mode interference devices based on self-imaging: principles and applications. J Lightwave Technol. 1995;13(4):615–27.

128. Zhang Y, et al. A compact and low loss Y-junction for submicron silicon waveguide. Opt Express. 2013;21(1):1310–6.
129. Yun H, Shi W, Wang Y, Chrostowski L, Jaeger N. 2x2 adiabatic 3-dB coupler on silicon-on-insulator rib waveguides. Proc SPIE. 2013;8915:89150V.
130. Xu L, et al. Compact high-performance adiabatic 3-dB coupler enabled by subwavelength grating slot in the silicon-on-insulator platform. Opt Express. 2018;26(23):29873–85.
131. Yun H, Chrostowski L, Jaeger N. Ultra-broadband 2 x 2 adiabatic 3 dB coupler using subwavelength-grating-assisted silicon-on-insulator strip waveguides. Opt Lett. 2018;43(8):1935–8.
132. Takagi A, Jinguji K, Kawachi M. Design and fabrication of broad-band silica-based optical waveguide couplers with asymmetric structure. IEEE J Quantum Electron. 1992;28(4):848–55.
133. Morino H, Maruyama T, Iiyama K. Reduction of wavelength dependence of coupling characteristics using Si optical waveguide curved directional coupler. J Lightwave Technol. 2014;32(12):2188–92.
134. Hsu S. Signal power tapped with low polarization dependence and insensitive wavelength on silicon-on-insulator platforms. J Opt Soc Am B. 2010;27(5):941–7.
135. Alam M, Caspers J, Aitchison J, Mojahedi M. Compact low loss and broadband hybrid plasmonic directional coupler. Opt Express. 2013;21(13):16029–34.
136. Lu Z, et al. Broadband silicon photonic directional coupler using asymmetric-waveguide based phase control. Opt Express. 2015;23(3):3795–806.
137. Gupta R, Chandran S, Das B. Wavelength-independent directional couplers for integrated silicon photonics. J Lightwave Technol. 2017;35(22):4916–23.
138. Halir R, et al. Colorless directional coupler with dispersion engineered sub-wavelength structure. Opt Express. 2012; 20(12):13470.
139. Wang Y, et al. Compact broadband directional couplers using subwavelength gratings. IEEE Photonics J. 2016;8(3):1–8.
140. Ye C, Dai D. Ultra-compact broadband 2×2 3dB power splitter using subwavelength-grating-assisted asymmetric directional coupler. IEEE J Lightw Technol. 2020;38:2370–5.
141. Lu L, Zhang M, and Liu D. Polarization insensitive 3-dB directional coupler based on sub-wavelength grating structure. Asia Communications and Photonics Conference. Optical Society of America, 2015.
142. Benedikovic D, et al. Sub-decibel silicon grating couplers based on L-shaped waveguides and engineered subwavelength metamaterials. Opt Express. 2019;27(18):26239–50.
143. Luque G, et al. An ultracompact GRIN-lens-based spot size converter using subwavelength grating metamaterials. Laser Photonics Rev. 2019;13(11):1900172.
144. Xu P, et al. SiN x–Si interlayer coupler using a gradient index metamaterial. Opt Lett. 2019;44(5):1230–3.
145. Papes M, et al. Fiber-chip edge coupler with large mode size for silicon photonic wire waveguides. Opt Express. 2016; 24(5):5026–38.
146. Ortega-Moñux A, et al. Disorder effects in subwavelength grating metamaterial waveguides. Opt Express. 2017;25(11): 12222–36.
147. Barwicz T. An O-band metamaterial converter interfacing standard optical fibers to silicon nanophotonic waveguides. In: Proc. Opt. Fiber Commun. Conf., 2015; Paper Th3F.3.
148. Barwicz T, Kamlapurkar S, Martin Y, Bruce R, and Engelmann S. A silicon metamaterial chip-to-chip coupler for photonic flip-chip applications. In Proc. Opt. Fiber Commun. Conf., 2017, Paper Th2A.39.
149. Picard M, Painchaud Y, Latrasse C, Larouche C, Pelletier F, and Poulin M. Novel spot-size converter for optical fiber to sub-μm silicon waveguide coupling with low loss, low wavelength dependence and high tolerance to alignment. in Proc. Eur. Conf. Opt. Commun. (ECOC), 2015;1–3.
150. Zhou W, et al. Subwavelength engineering in silicon photonic devices. IEEE J Select Top Quantum Electron. 2019; 25(3):1–13.
151. Taillaert D, et al. An out-of-plane grating coupler for efficient buttcoupling between compact planar waveguides and single-mode fibers. IEEE J Quantum Electron. 2002;38(7):949–55.
152. Topley R, et al. Locally erasable couplers for optical device testing in silicon on insulator. J Lightwave Technol. 2014; 32(12):2248–53.
153. Chen X, et al. Post-fabrication phase trimming of Mach–Zehnder interferometers by laser annealing of germanium implanted waveguides. Photon Res. 2017;5(6):578–82.
154. Milosevic M, et al. Ion implantation in silicon for trimming the operating wavelength of ring resonators. IEEE J Sel Topics Quantum Electron. 2018;24(4):8200107.
155. Li C, et al. Silicon photonics packaging with lateral fiber coupling to apodized grating coupler embedded circuit. Opt Express. 2014;22(20):24235–40.
156. Tong Y, Zhou W, Tsang HK. Efficient perfectly vertical grating coupler for multi-core fibers fabricated with 193 nm DUV lithography. Opt Lett. 2018;43(23):5709–12.
157. Taillaert D, et al. A compact two-dimensional grating coupler used as a polarization splitter. IEEE Photon Technol Lett. 2003;15(9):1249–51.
158. Watanabe T, Ayata M, Koch U, Fedoryshyn Y, Leuthold J. Perpendicular grating coupler based on a blazed antiback-reflection structure. J Lightwave Technol. 2017;35(21):4663–9.
159. Chen X, Li C, Tsang HK. Fabrication-tolerant waveguide chirped grating coupler for coupling to a perfectly vertical optical fiber. IEEE Photon Technol Lett. 2008;20(23):1914–6.
160. Roelkens G, Van Thourhout D, Baets R. Silicon-on-insulator ultra-compact duplexer based on a diffractive grating structure. Opt Express. 2007;15(16):10091–6.
161. Xu L, Chen X, Li C, Tsang HK. Bi-wavelength two-dimensional chirped grating couplers for low cost WDM PON transceivers. Opt Commun. 2011;284(8):2242–4.
162. Piggott A, et al. Inverse design and implementation of a wavelength demultiplexing grating coupler. Sci Rep. 2014;4: 7210.
163. Ding Y, et al. On-chip grating coupler array on the SOI platform for fan-in/fan-out of MCFs with low insertion loss and crosstalk. Opt Express. 2015;23(3):3292–8.

164. Chen X, Tsang HK. Nanoholes grating couplers for coupling between silicon-on-insulator waveguides and optical fibers. IEEE Photon J. 2009;1(3):184–90.
165. Chen X, Xu K, Cheng Z, Fung C, Tsang HK. Wideband subwavelength gratings for coupling between silicon-on-insulator waveguides and optical fibers. Opt Lett. 2012;37(17):3483–5.
166. Cheng Z, Chen X, Wong CY, Xu K, Tsang HK. Apodized focusing subwavelength grating couplers for suspended membrane waveguides. Appl Phys Lett. 2012;101(10):101104.
167. Cheng Z, Chen X, Wong CY, Xu K, Tsang HK. Broadband focusing grating couplers for suspended-membrane waveguides. Opt Lett. 2012;37(24):5181–3.
168. Cheng Z, et al. Focusing subwavelength grating coupler for midinfrared suspended membrane waveguide. Opt Lett. 2012;37(7):1217–9.
169. Cheng Z, Tsang HK. Experimental demonstration of polarization insensitive air-cladding grating couplers for silicon-on-insulator waveguides. Opt Lett. 2014;39(7):2206–9.
170. Cheng Z, Chen X, Wong CY, Xu K, Tsang HK. Midinfrared suspended membrane waveguide and ring resonator on siliconon-insulator. IEEE Photon J. 2012;4(5):1510–9.
171. Cheben P, et al. Subwavelength waveguide grating for mode conversion and light coupling in integrated optics. Opt Express. 2006;14(11):4695–702.
172. Cheben P, et al. Refractive index engineering with subwavelength gratings for efficient microphotonic couplers and planar waveguide multiplexers. Opt Lett. 2010;35(15):2526–8.
173. Cheben P, et al. Broadband polarization independent nanophotonic coupler for silicon waveguides with ultra-high efficiency. Opt Express. 2015;23(17):22553–63.
174. Dai D, et al. 10-channel mode (de) multiplexer with dual polarizations. Laser Photonics Rev. 2018;12(1):1700109.
175. Uematsu T, et al. Design of a compact two-mode multi/demultiplexer consisting of multimode interference waveguides and a wavelength-insensitive phase shifter for mode-division multiplexing transmission. J Lightwave Technol. 2012; 30(15):2421–6.
176. Driscoll J, et al. Asymmetric Y junctions in silicon waveguides for on-chip mode-division multiplexing. Opt Lett. 2013; 38(11):1854–6.
177. Chen W, Wang P, Yang J. Mode multi/demultiplexer based on cascaded asymmetric Y-junctions. Opt Express. 2013; 21(21):25113–9.
178. Frellsen L, et al. Topology optimized mode multiplexing in silicon-on-insulator photonic wire waveguides. Opt Express. 2016;24(15):16866–73.
179. Xing J, et al. Two-mode multiplexer and demultiplexer based on adiabatic couplers. Opt Lett. 2013;38(17):3468–70.
180. Li C, Dai D. Low-loss and low-crosstalk multi-channel mode (de) multiplexer with ultrathin silicon waveguides. Opt Lett. 2017;42(12):2370–3.
181. Guo D, Chu T. Silicon mode (de) multiplexers with parameters optimized using shortcuts to adiabaticity. Opt Express. 2017;25(8):9160–70.
182. Sun C, et al. Silicon mode multiplexer processing dual-path mode-division multiplexing signals. Opt Lett. 2016;41(23): 5511–4.
183. Greenberg M, Orenstein M. Multimode add-drop multiplexing by adiabatic linearly tapered coupling. Opt Express. 2005; 13(23):9381–7.
184. Ding Y, et al. On-chip two-mode division multiplexing using tapered directional coupler-based mode multiplexer and demultiplexer. Opt Express. 2013;21(8):10376–82.
185. Dai D, Wang J, Shi Y. Silicon mode (de) multiplexer enabling high capacity photonic networks-on-chip with a single-wavelength-carrier light. Opt Lett. 2013;38(9):1422–4.
186. Qiu H, et al. Silicon mode multi/demultiplexer based on multimode grating-assisted couplers. Opt Express. 2013;21: 17904–11.
187. He Y, Zhang Y, Zhu Q, An S, et al. Silicon high-order mode (De)multiplexer on single polarization. IEEE/OSA J Lightw Technol. 2018;36(24):5746–53.
188. Mehrabi K, Zarifkar A. Ultracompact and ultrabroadband mode division multiplexer based on an Au nanocube array assisted directional coupler. Appl Opt. 2020;59(5):1286–92.
189. Jiang W, et al. On-chip silicon dual-mode multiplexer via a subwavelength grating-based directional coupler and a mode blocker. Appl Opt. 2019;58(33):9290–6.
190. Dave U, and Lipson M. Efficient conversion to very high order modes in silicon waveguides. CLEO: Science and Innovations. Optical Society of America, 2019.
191. Li C, Ye C, and Dai D. SWG-assisted multimode add-drop multiplexer. (to be submitted)
192. Jiang W, et al. Ultrabroadband and fabrication-tolerant mode (de) multiplexer using subwavelength structure. JOSA B. 2019;36(11):3125–32.
193. Jiang W, Wang X. Ultra-broadband mode splitter based on phase controlling of bridged subwavelength grating. J Lightwave Technol. 2020;99:1–1.
194. Park J, Yeo D, Shin S. Variable optical mode generator in a multimode waveguide. IEEE Photon Technol Lett. 2006; 18(20):2084–6.
195. Huang Y, Xu G, Ho S. An ultracompact optical mode order converter. IEEE Photon Technol Lett. 2006;18(21):2281–3.
196. Chen D, et al. Low-loss and fabrication tolerant silicon mode-order converters based on novel compact tapers. Opt Express. 2015;23:11152–9.
197. Molesky S, et al. Inverse design in nanophotonics. Nat Photonics. 2018;12(11):659.
198. Liu V, et al. Ultra-compact photonic crystal waveguide spatial mode converter and its connection to the optical diode effect. Opt Express. 2012;20(27):28388–97.
199. Lu J, Vuckovic J. Nanophotonic computational design. Opt Express. 2013;21(11):13351–67.
200. Shen B, Polson R, Menon R. Integrated digital metamaterials enable ultra-compact optical diodes. Opt Express. 2015; 23(8):10847–55.
201. Yu Z, Cui H, Sun X. Genetic-algorithm-optimized wideband on-chip polarization rotator with an ultrasmall footprint. Opt Lett. 2017;42(16):3093–6.

202. Frandsen L, et al. Topology optimized mode conversion in a photonic crystal waveguide fabricated in silicon-on-insulator material. Opt Express. 2014;22(7):8525–32.
203. Frellsen L, Ding Y, Sigmund O, and Frandsen L. Topology-optimized mode converter in a silicon-on-insulator photonic wire waveguide. CLEO: Science and Innovations. Optical Society of America, 2016; STh3E. 4.
204. Jia H, et al. Inverse-design and demonstration of ultracompact silicon meta-structure mode exchange device. ACS Photon. 2018;5:1833–8.
205. Ohana D, et al. Dielectric metasurface as a platform for spatial mode conversion in nanoscale waveguides. Nano Lett. 2016;16(12):7956–61.
206. Li Z, et al. Controlling propagation and coupling of waveguide modes using phase-gradient metasurfaces. Nat Nanotechnol. 2017;12(7):675.
207. Luque-González J, et al. Tilted subwavelength gratings: controlling anisotropy in metamaterial nanophotonic waveguides. Opt Lett. 2018;43(19):4691–4.
208. Yao C, et al. Multi-mode conversion via two-dimensional refractive-index perturbation on a silicon waveguide. arXiv preprint arXiv. 2019; 1911.10786.
209. Wang T, et al. Ultra-compact reflective mode converter based on a silicon subwavelength structure. Appl Opt. 2020; 59(9):2754–8.
210. Cheng Z, et al. Sub-wavelength grating assisted mode order converter on the SOI substrate. Opt Express. 2019;27(23): 34434–41.
211. González-Andrade D, et al. Ultra-broadband mode converter and multiplexer based on sub-wavelength structures. IEEE Photonics J. 2018;10(2):1–10.
212. Chen R, et al. Ultra-compact hybrid plasmonic mode convertor based on unidirectional eigenmode expansion. Opt Lett. 2020;45(4):803–6.
213. Wang H, Zhang Y, He Y, Zhu Q, Sun L, Su Y. Compact silicon waveguide mode converter employing dielectric metasurface structure. Adv Opt Mater. 2019;7(4):1801191.
214. Guo J, et al. Extremely compact guided-mode exchangers on silicon. Laser Photonics Rev. 2020;202000058.
215. Luo Y, Yu Y, Ye M, Sun C, Zhang X. Integrated dual-mode 3 dB power coupler based on tapered directional coupler. Sci Rep. 2016;6:23516.
216. Xu H, Shi Y. Ultra-broadband dual-mode 3 dB power splitter based on a Y-junction assisted with mode converters. Opt Lett. 2016;41(21):5047–50.
217. Han L, Kuo B, Alic N, Radic S. Ultra-broadband multimode 3dB optical power splitter using an adiabatic coupler and a Y-branch. Opt Express. 2018;26(11):14800–9.
218. Chang W, et al. Inverse design and demonstration of an ultracompact broadband dual-mode 3 dB power splitter. Opt Express. 2018;26(18):24135–44.
219. Xie H, et al. An ultra-compact 3-dB power splitter for three modes based on pixelated meta-structure. IEEE Photon Technol Lett. 2020;32(6):341–4.
220. Ye C, Dai D. Broadband dual-mode 2×2 3 dB power splitter based on multimode interference couplers with shallowly etched subwavelength gratings. Appl Opt. 2020;59:7308–12.
221. Erol A, Sözüer H. High transmission through a 90° bend in a polarization-independent single-mode photonic crystal waveguide. Opt Express. 2015;23(25):32690–5.
222. Shen B, Polson R, Menon R. Metamaterial-waveguide bends with effective bend radius< λ 0/2. Opt Lett. 2015;40(24): 5750–3.
223. Fujisawa T, et al. Low-loss, compact, and fabrication-tolerant Si-wire 90° waveguide bend using clothoid and normal curves for large scale PICs. Opt Express. 2017;25(8):9150–9.
224. Cherchi M, et al. Dramatic size reduction of waveguide bends on a micron-scale silicon photonic platform. Opt Express. 2013;21(15):17814–23.
225. Yuanyuan C, et al. Analysis on influencing factors of bend loss of silicon-on-insulator waveguides. J Semicond. 2005;26:216.
226. Gabrielli L, et al. On-chip transformation optics for multimode waveguide bends. Nat Commun. 2012;3:1217.
227. Dai D. Multimode optical waveguide enabling microbends with low inter-mode crosstalk for mode-multiplexed optical interconnects. Opt Express. 2014;22:27524–34.
228. Dai D, Wang J, He S. Silicon multimode photonic integrated devices for on-chip mode-division-multiplexed optical interconnects. Prog Electromagn Res. 2013;143:773–819.
229. Wu X, et al. Low crosstalk bent multimode waveguide for on-chip mode-division multiplexing interconnects. //CLEO: QELS_Fundamental Science. Optical Society of America, 2018; JW2A. 66.
230. Jiang X, Wu H, Dai D. Low-loss and low-crosstalk multimode waveguide bend on silicon. Opt Express. 2018;26:17680–9.
231. Sun C, et al. A novel sharply bent silicon multimode waveguide with ultrahigh mode ER. Optical Fiber Communications Conference and Exhibition. IEEE, 2016.
232. Sun C, Yu Y, Chen G, Zhang X. Ultra-compact bent multimode silicon waveguide with ultralow inter-mode crosstalk. Opt Lett. 2017;42(15):3004–7.
233. Xu H, Shi Y. Ultra-sharp multi-mode waveguide bending assisted with metamaterial-based mode converters. Laser Photonics Rev. 2018;12:1700240.
234. Teng M, et al. A 3-micron-radius bend for SOI TE0/TE1 multiplexing //CLEO: applications and technology. Optical Society of America, 2018: JW2A. 13.
235. Chang W, et al. Ultra-compact silicon multi-mode waveguide bend based on subwavelength asymmetric Y-junction. Optical Fiber Communication Conference. Optical Society of America 2018: Tu3A. 1
236. Liu Y, et al. Very sharp adiabatic bends based on an inverse design. Opt Lett. 2018;43(11):2482–5.
237. Wu H, et al. Ultra-sharp multimode waveguide bends with subwavelength gratings. Laser Photonics Rev. 2019;13(2): 1800119.
238. Xie H, et al. Demonstration of an ultra-compact bend for four modes based on pixelated meta-structure. Optical Fiber Communication Conference. Optical Society of America, 2020.
239. Wang Y, Dai D. Ultra-sharp multimode waveguide bends with dual polarizations. J Lightwave Technol. 2020;38(15): 3994–9.

240. Chen H, Poon A. Low-loss multimode-interference-based crossings for silicon wire waveguides. IEEE Photon Technol Lett. 2006;18(21):2260–2.
241. Bogaerts W, et al. Low-loss, low-cross-talk crossings for silicon-on-insulator nanophotonic waveguides. Opt Lett. 2007; 32(19):2801–3.
242. Kim S-H, et al. Low-crosstalk waveguide crossing based on 1×1 MMI structure of silicon-wire waveguide. 2013 Conference on Lasers and Electro-Optics Pacific Rim (CLEOPR). IEEE, 2013.
243. Liu Y, et al. Ultra-low-loss CMOS-compatible waveguide crossing arrays based on multimode Bloch waves and imaginary coupling. Opt Lett. 2014;39(2):335–8.
244. Zhang Y, et al. Ultralow-loss silicon waveguide crossing using Bloch modes in index-engineered cascaded multimode-interference couplers. Opt Lett. 2013;38(18):3608–11.
245. Bock P, et al. Subwavelength grating crossings for silicon wire waveguides. Opt Express. 2010;18(15):16146–55.
246. Sun C, Yu Y, Zhang X. Ultra-compact waveguide crossing for a mode-division multiplexing optical network. Opt Lett. 2017;42(23):4913–6.
247. Chang W, et al. An ultracompact multimode waveguide crossing based on subwavelength asymmetric Y-junction. IEEE Photonics J. 2018;10(4):1–8.
248. Chang W, et al. Ultracompact dual-mode waveguide crossing based on subwavelength multimode-interference couplers. Photonics Res. 2018;6(7):660–5.
249. Xu H, Shi Y. Dual-mode waveguide crossing utilizing taper-assisted multimode-interference couplers. Opt Lett. 2016; 41(22):5381–4.
250. Chang W, Zhang M. Silicon-based multimode waveguide crossings. J Phys Photonics. 2020;2(2):022002.
251. Xu H, Shi Y. Metamaterial-based Maxwell's fisheye lens for multimode waveguide crossing. Laser Photonics Rev. 2018; 12(10):1800094.
252. Chen LR, et al. Subwavelength grating waveguide devices for telecommunications applications. IEEE J Sel Top Quant Electron. 2018;25(3):8200111.
253. Wang J, Glesk I, Chen L. Subwavelength grating Bragg grating filters in silicon-on-insulator. IET Electron Lett. 2015;51(9): 712–3.
254. Pérez-Galacho D, et al. Optical pump-rejection filter based on silicon sub-wavelength engineered photonic structures. Opt Lett. 2017;42(8):1468–71.
255. Sumi R, et al. Ultra-broadband add-drop filter/switch circuit using subwavelength grating waveguides. IEEE J Select Top Quantum Electron. 2018;25(3):1–11.
256. Chen J, Shi Y. Flat-top CWDM (De) multiplexers based on contra-directional couplers with subwavelength gratings. IEEE Photon Technol Lett. 2019;31(24):2003–6.
257. Ma K, Han S, Long Z, et al. Optical forces in silicon subwavelength-grating waveguides. Opt Express. 2017;25(25):30876.
258. Huang L, et al. Improving the detection limit for on-chip photonic sensors based on subwavelength grating racetrack resonators. Opt Express. 2017;25(9):10527–35.
259. Zhang L, Dai D. Silicon subwavelength-grating microdisks for optical sensing. IEEE Photon Technol Lett. 2019;31(15): 1209–12.
260. Flueckiger J, et al. Subwavelength grating for enhanced ring resonator biosensor. Opt Express. 2016;24(14):15672–86.
261. Pan Z, et al. High-speed modulator based on electro-optic polymer infiltrated subwavelength grating waveguide ring resonator. Laser Photonics Rev. 2018;12(6):1700300.
262. Abdelatty M, Swillam MA. Hybrid plasmonic electro-optical absorption modulator based on phase change characteristics of vanadium-dioxide. J Nanophotonics. 2019;13(4):046014.
263. Jean P, et al. Slow light in subwavelength grating waveguides. IEEE J Select Top Quantum Electron. 2019;26(2):8200108.
264. Gervais A, et al. Tunable slow-light in silicon photonic subwavelength grating waveguides. 2019 IEEE 16th International Conference on Group IV Photonics (GFP). IEEE, 2019.
265. Wang J, et al. Subwavelength grating enabled on-chip ultra-compact optical true time delay line. Sci Rep. 2016;6:30235.
266. Li T, and Zou Y. Coupling condition engineered subwavelength grating waveguide ring resonator for sensitivity enhancement. Integrated Optics: Devices, Materials, and Technologies XXIV. Vol. 11283. International Society for Optics and Photonics, 2020.
267. Glesk I, et al. All-optical switching using nonlinear subwavelength Mach-Zehnder on silicon. Opt Express. 2011;19(15): 14031–9.
268. Babaei M, et al. Compact and broadband 2× 2 optical switch based on hybrid plasmonic waveguides and curved directional couplers. Appl Opt. 2020;59(4):975–84.
269. Glesk I, et al. Picosecond all-optical switching using nonlinear Mach–Zehnder with silicon subwavelength grating and photonic wire arms. Opt Quant Electron. 2012;44(12-13):613–21.
270. Bock P, et al. Subwavelength grating Fourier-transform interferometer array in silicon-on-insulator. Laser Photonics Rev. 2013;**7**(6):L67–70.
271. González-Andrade D, et al. Ultra-broadband nanophotonic phase shifter based on subwavelength metamaterial waveguides. Photonics Res. 2020;8(3):359–67.

Publisher's Note